Analysis of transversely isotropic compressible and nearly-incompressible soft material structures by high order unified finite elements

(Article begins on next page)

01 August 2024

# Analysis of transversely isotropic compressible and nearly-incompressible soft material structures by high order unified finite elements

P. Chiaia[a]*, A. Pagani[a]†, M. Cinefra[b]‡, E. Carrera[a]§

*a* Mul² Lab, Department of Mechanical and Aerospace Engineering
Politecnico di Torino, 10129 Turin, Italy
*b* Department of Mechanics, Mathematics and Management, Politecnico di Bari
Via Edoardo Orabona, 4, 70126 Bari, Italy

**Abstract** *This work proposes high-order beam (1D) and plate (2D) finite element models for the large strain analysis of compressible and incompressible transversely isotropic hyperelastic media, defined within the Carrera Unified Formulation (CUF) framework. The strain energy density function adopted in fiber-reinforced hyperelastic materials modeling is presented and expressed in terms of invariants and pseudo-invariants of the right Cauchy-Green strain tensor. The explicit expression of the tangent elasticity tensor is derived through the assumption of coupled formulation of strain energy functions. Refined fully nonlinear beam and plate models are defined in a total Lagrangian formulation, deriving the governing equations of the nonlinear static analysis through the Principle of Virtual Displacements in terms of fundamental nuclei, in resulting expressions of internal and external forces vectors, and tangent stiffness matrix independent of kinematic models and approximation theories adopted. The iterative Newton-Raphson linearization scheme coupled with the arc-length constraint is adopted to obtain actual numerical solutions. Different benchmark analyses in hyperelasticity are performed to assess the capabilities of our proposed model, analyzing the three-dimensional stress field for moderate to large strain states and comparing actual numerical results with exact closed-form solutions or results available in the literature, demonstrating the capabilities and reliability of CUF models in the analysis of fiber-reinforced soft materials and structures.*

**Keywords** Hyperelasticity; Fiber-reinforced hyperelastic materials; Soft structures; Unified Formulation; Compressible hyperelastic models; Path-following methods.

## 1 Introduction

Bio-inspired material, soft rubber-like cross-ply, or multilayered biological tissues have been subjected to intense studies in the last decades. Of particular relevance, the numerical simulation of mechanical behavior of soft tissue is an actual challenging field in computational mechanics and fluid dynamics since it allows a wide range of investigations to better understand the real nature of biological tissues. In this framework, materials involved in muscular and cardiac tissue modeling deal with strong anisotropy. Typically these are multilayered materials, and each sub-layer exhibits direction-dependent mechanical properties and typical of fiber-reinforced materials, such as collagen fibers, muscular tissue,

---

*PhD student. E-mail piero.chiaia@polito.it
†Associate Professor. E-mail alfonso.pagani@polito.it
‡Associate Professor. E-mail maria.cinefra@poliba.it
§Professor of Aerospace Structures and Aeroelasticity. E-mail erasmo.carrera@polito.it

and blood vessels. For such materials, the mechanical behavior is described by transversely isotropic hyperelastic constitutive law, for which direction-dependent mechanical properties are taken into account.

The enhanced elastic properties given by the hyperelastic behavior and the microstructural fiber-reinforcement are the key properties of biological tissue. Fok *et al.* [1] analyzed multilayered arterial cross-section by morpho-elasticity arguments. Holzapfel *et al.* [2] presented one of the most accurate hyperelastic models in biological tissue modeling, the HGO (Holzapfel-Gasser-Ogden) model, considering transversely isotropic and orthotropic hyperelasticity, presenting a novel constitutive law for arterial tissue modeling. A mathematical treatment of pseudoelastic stress-strain relations in hyperelasticity has been presented by Fung *et al.* [3]. Some of the most remarkable hyperelastic models for rubber and biological tissues have been validated by Ogden [4] and Gent [5], the last one later analyzed also by Puglisi *et al.* [6].

In a general scenario, constitutive equations for anisotropic hyperelastic materials are well-established transversely isotropic and orthotropic hyperelastic constitutive models are defined including large displacements and strains formulation and a nonlinear stress-strain relation, both embedded in the classical strain energy function approach to hyperelastic material modeling. The availability of mathematical models of hyperelastic materials allows the implementation of numerical procedures for simulations of biological tissues. Due to the strongly nonlinear behavior of mathematical models, analytical solutions are few and limited to very simple cases; for this reason, numerical procedures based on Finite Element Method are one of the most common approaches. Arbind *et al.* [7] presented a general higher-order shell theory for compressible hyperelastic materials. Amabili *et al.* [8] presented a finite element model based on higher-order shell theories for the analysis of biological materials. Also Amabili *et al.* [9] presented some experimental and numerical results on the characterization of human aortas. Thin fiber-reinforced hyperelastic shells based on Reissner-Mindlin kinematics have been analyzed by Balzani *et al.* [10]. Fiber-reinforced elastomers and their characterization by classical tension test have been studied in a finite element scenario by Brown *et al.* [11]. Canales *et al.* [12] presented a nonlinear optimization algorithm in the characterization of mechanical properties possessed by anisotropic hyperelastic behavior modeled with the HGO model. Beheshti *et al.* [13] presented a general high-order shell model for the analysis of compressible transversely isotropic materials. Zdunek *et al.* [14] proposed a hybrid finite element formulation for transversely isotropic hyperelasticity.

In this work, we propose a new general finite element formulation for the analysis of transversely isotropic (or continuous fiber-reinforced) hyperelastic materials based on Carrera Unified Formulation (CUF). In this framework, the three-dimensional displacement field is expressed in terms of a recursive index notation coupling kinematic models and approximation theories along the cross-section (1D beam models) or thickness (2D plate/shell models), allowing the definition of matrix-form physical quantities appearing in nonlinear governing equations in terms of fundamental nuclei independent of the polynomial approximation employed in the definition of the finite element. The theoretical framework of CUF and the definition oh higher-order structural theories is presented in Carrera *et al.* [15]. The accuracy of CUF models in the computation of accurate three-dimensional stress distributions is established in many works as [16, 17, 18]. Higher-order CUF models have been extended more recently to the geometrical nonlinear analysis of isotropic and composite structures [19, 20, 21] but more recently the material nonlinearities of the hyperelastic constitutive law has been included in the fully nonlinear beam, plate and hexahedral solid models as done in [22, 23, 24].

The present work is structured as follows (i) first, the mathematical formulations of kinematics, hyperelastic constitutive law written under an invariant formulation and the tangent elasticity tensor are presented in Section 2.1; (ii) second, unified CUF-based 1D and 2D models are discussed in Section 3; (iii) subsequently, we exploit the nonlinear governing equations by means of the Principle of Virtual Displacements, defining the internal and external forces vector and tangent stiffness matrix fundamental nuclei, presenting also the numerical iterative scheme employed in Section 4; (iv) numerical results obtained by the present implementation of unified beam and plated models are presented in Section 5, establishing the capabilities of the present models in the case of compressible and incompressible fiber-reinforced materials; (v) finally, we discuss about the main conclusions evinced in Section 6.

## 2 Constitutive law

### 2.1 Kinematics and strain measures

Figure 1 shows the undeformed $\mathbf{\Omega_0}$ and deformed configuration $\mathbf{\Omega}$ of a continuum body in space, where $P_0 = (x^0, y^0, z^0)$ stands for a material point in the undeformed configuration and $P$ the associated point in the actual deformed configuration. As the continuum body evolves during time, it occupies a continuous sequence of regions of the euclidean space. These regions occupied by the body at a certain time $t$ are the *configurations* of the body. Starting from the reference configuration $\mathbf{\Omega_0}$, the configuration of the body at the generic instant $t$ is called the *current configuration*.
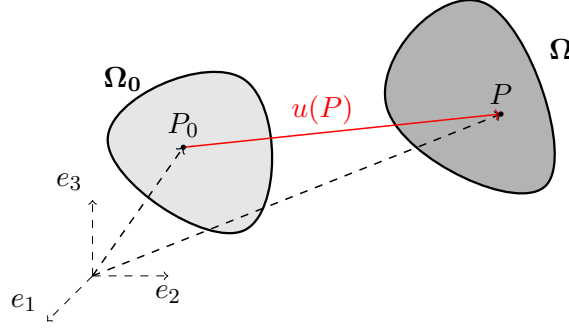


**Figure 1:** Reference and actual configuration of a deformable body.

The current position of the generic material point is described by the *deformation function*, that maps material point in the actual configuration to the related position in the reference configuration

$$\mathbf{P} = \mathbf{f}(\mathbf{P_0}) = x\mathbf{e_1} + y\mathbf{e_2} + z\mathbf{e_3} = f_1(x^0, y^0, z^0)\mathbf{e_1} + f_2(x^0, y^0, z^0)\mathbf{e_2} + f_3(x^0, y^0, z^0)\mathbf{e_3} \tag{1}$$

thereafter, the classical strain measures commonly adopted in continuum mechanics, namely the deformation gradient $\mathbf{F} = \partial \mathbf{P}/\partial \mathbf{P_0}$ and the right Cauchy-Green strain tensor $\mathbf{C} = \mathbf{F}^T\mathbf{F}$, are automatically defined. Typically, isotropic hyperelastic mathematical models are defined starting from the invariants of the right Cauchy-Green strain tensor, to satisfy objectivity arguments and independence with respect to the reference frame, referring then to

$$I_1 = \text{tr}(\mathbf{C}) \tag{2}$$

$$I_2 = \frac{1}{2}((\text{tr}(\mathbf{C}))^2 - \text{tr}(\mathbf{C}^2)) = \text{tr}(\text{cof}(\mathbf{C})) \tag{3}$$

$$I_3 = \det(\mathbf{C}) = \det(\mathbf{F}^T\mathbf{F}) = J^2 \tag{4}$$

where $\text{tr}(\cdot)$ and $\det(\cdot)$ are the trace and the determinant operators, and $\text{cof}(\cdot)$ is the matrix of the cofactors. Hyperelastic anisotropy is studied by analyzing the mechanical behavior of the material when direction-dependent constitutive laws are provided. In this work, fiber-reinforced materials (transversely isotropic materials) will be considered. For such materials, supposing that $\mathbf{a_0} = (a_x, a_y, a_z)^T$ is the single fiber-reinforcement direction, the dependence on the preferential direction of the mechanical response is embedded in the model considering two additional *pseudo-invariants* [25]

$$I_4 = \mathbf{a_0} \cdot \mathbf{Ca_0} \tag{5}$$

$$I_5 = \mathbf{a_0} \cdot \mathbf{C}^2\mathbf{a_0} \tag{6}$$

One can note that $I_4$ and $I_5$ are invariants only under a rotation with the respect of fiber axis.

## 2.2 Hyperelastic constitutive law in terms of invariants

The mechanical behavior of continuously fiber-reinforced soft materials is modeled in the classical hyperelastic framework based on strain energy functions. Considering a transversely isotropic hyperelastic material, the classical strain energy function $\Psi$ for isotropic materials (depending on the invariants $(I_1, I_2, I_3)$ of right Cauchy-Green tensor $\mathbf{C}$) is extended embedding the dependence on the preferential direction is embedded in the definition. If, in a Cartesian reference frame, the vector of the fiber direction is $\mathbf{a_0} = (a_x, a_y, a_z)^T$, the strain energy function is now expressed as a function of two tensorial quantities

$$\Psi = \Psi(\mathbf{C}, \mathbf{a_0} \otimes \mathbf{a_0}) \tag{7}$$

where $(\cdot) \otimes (\cdot)$ stands for the dyadic product (tensor product) operator. The dependence on the special direction of the continuous fiber-reinforcement is expressed, in the three-dimensional space, by the structural tensor $\mathbf{a_0} \otimes \mathbf{a_0}$ that modifies the constitutive equation. Due to the independence of the strain energy function with respect to the reference frame (objectivity argument), $\Psi$ is expressed as a function of the three classical principal invariants of $\mathbf{C}$ and two additional *pseudo-invariants*, in which the dependence of the fiber-reinforcement direction is incorporated and objectivity is still verified

$$\Psi = \Psi(I_1(\mathbf{C}), I_2(\mathbf{C}), I_3(\mathbf{C}), I_4(\mathbf{C}, \mathbf{a_0}), I_5(\mathbf{C}, \mathbf{a_0})) \tag{8}$$

In nearly-incompressible hyperelastic materials, the volume ratio coefficient defined as $J = \det(\mathbf{F})$ is approaching the unity, thus also $I_3$.

In literature, commonly adopted models refer to the *decoupled* formulation of strain energy functions, namely $\Psi$ is written as the sum of a purely volumetric component, a purely isochoric component, and an additional anisotropic one

$$\Psi = \Psi_{vol}(J) + \bar{\Psi}_{iso}(\bar{I}_1, \bar{I}_2) + \bar{\Psi}_{aniso}(\bar{I}_1, \bar{I}_2, \bar{I}_4, \bar{I}_5) \tag{9}$$

where $\bar{\Psi}_{iso}$ and $\bar{\Psi}_{aniso}$ depend on the rescaled isotropic invariants, namely invariants $(\bar{I}_1, \bar{I}_2, \bar{I}_3)$ of $\bar{\mathbf{C}} = J^{-2/3}\mathbf{C}$ and anisotropic rescaled invariants $\bar{I}_4 = J^{-2/3}I_4$ and $\bar{I}_5 = J^{-4/3}I_5$. For a more detailed description of the model see Holzapfel [25].

In our model, to simulate materials modeled with any possible strain energy function models, the expression of $\Psi$ Eq.(8) is assumed. The constitutive law for transversely isotropic material is carried out by classical hyperelastic arguments. Once assigned the strain energy function, the stress-strain relation adopted is

$$\mathbf{S} = 2\frac{\partial \Psi(\mathbf{C})}{\partial \mathbf{C}} \tag{10}$$

where $\mathbf{S}$ is the PK2 (Piola-Kirchoff-2) stress tensor. Applying now the chain rule, the derivative of $\Psi$ with respect to $\mathbf{C}$ can be explicitly expressed as

$$\frac{\partial \Psi(\mathbf{C})}{\partial \mathbf{C}} = \frac{\partial \Psi(\mathbf{C})}{\partial I_1}\frac{\partial I_1}{\partial \mathbf{C}} + \frac{\partial \Psi(\mathbf{C})}{\partial I_2}\frac{\partial I_2}{\partial \mathbf{C}} + \frac{\partial \Psi(\mathbf{C})}{\partial I_3}\frac{\partial I_3}{\partial \mathbf{C}} + \frac{\partial \Psi(\mathbf{C})}{\partial I_4}\frac{\partial I_4}{\partial \mathbf{C}} + \frac{\partial \Psi(\mathbf{C})}{\partial I_5}\frac{\partial I_5}{\partial \mathbf{C}} \tag{11}$$

In this manner, the analytic expression of PK2 stress tensor is obtained by computing derivatives of $\Psi$ with respect to invariants of the deformation process, since the derivatives of the invariant with respect to $\mathbf{C}$ are easily computed starting from their definitions

$$\frac{\partial I_1}{\partial \mathbf{C}} = \frac{\partial \mathrm{tr}\mathbf{C}}{\partial \mathbf{C}} = \frac{\partial (\mathbf{IC})}{\partial \mathbf{C}} = \mathbf{I} \tag{12}$$

$$\frac{\partial I_2}{\partial \mathbf{C}} = \frac{1}{2}\left(\mathrm{tr}\mathbf{C}\,\mathbf{I} - \frac{\partial \mathrm{tr}\mathbf{C}^2}{\partial \mathbf{C}}\right) = I_1\mathbf{I} - \mathbf{C} \tag{13}$$

$$\frac{\partial I_3}{\partial \mathbf{C}} = I_3\mathbf{C}^{-1} \tag{14}$$

4

$$\frac{\partial I_4}{\partial \mathbf{C}} = \mathbf{a_0} \otimes \mathbf{a_0} \tag{15}$$

$$\frac{\partial I_5}{\partial \mathbf{C}} = \mathbf{a_0} \otimes \mathbf{C}\mathbf{a_0} + \mathbf{a_0}\mathbf{C} \otimes \mathbf{a_0} \tag{16}$$

Substituting above expressions into Eq.(11), the most general expression of PK2 stress tensor depending of the strain energy function is derived

$$\mathbf{S} = 2\left[\left(\frac{\partial \Psi}{\partial I_1} + I_1 \frac{\partial \Psi}{\partial I_2}\right)\mathbf{I} - \frac{\partial \Psi}{\partial I_2}\mathbf{C} + I_3 \frac{\partial \Psi}{\partial I_3}\mathbf{C}^{-1} + \frac{\partial \Psi}{\partial I_4}\mathbf{a_0} \otimes \mathbf{a_0} + \frac{\partial \Psi}{\partial I_5}\left(\mathbf{a_0} \otimes \mathbf{C}\mathbf{a_0} + \mathbf{a_0}\mathbf{C} \otimes \mathbf{a_0}\right)\right] \tag{17}$$

In Eq.(17) the explicit dependence of the constitutive law with respect to the preferential direction of the material is included by the additional terms referred to the derivatives with respect to $I_4$ and $I_5$.

## 2.3 Incremental formulation and tangent elasticity tensor

In a total Lagrangian formulation of geometrical and material nonlinear problems, incremental formulations are required. According to Holzapfel [25], the constitutive equation (17) can be rewritten in an incremental form

$$\Delta \mathbf{S} = \mathbb{C}\frac{1}{2}\Delta \mathbf{C} \tag{18}$$

where $\mathbb{C}$ is the well-known material Jacobian tensor or tangent elasticity tensor. In the linearized version of governing equation

$$\mathbb{C} = 2\frac{\partial \mathbf{S}(\mathbf{C})}{\partial \mathbf{C}} = \frac{\partial \mathbf{S}(\mathbf{E})}{\partial \mathbf{E}} = 4\frac{\partial^2 \Psi}{\partial \mathbf{C}\partial \mathbf{C}} \tag{19}$$

Thereafter, by exploiting the derivatives of the strain energy function, one can obtain the analytic closed-form expression of the tangent elasticity tensor here presented

$$
\begin{aligned}
\mathbb{C} = & \ 4\left(\frac{\partial^2 \Psi}{\partial I_1^2} + 2I_1 \frac{\partial^2 \Psi}{\partial I_1 \partial I_2} + \frac{\partial \Psi}{\partial I_2} + I_1^2 \frac{\partial^2 \Psi}{\partial I_2^2}\right)\mathbf{I} \otimes \mathbf{I} + 4\left(\frac{\partial^2 \Psi}{\partial I_1 \partial I_2} + I_1 \frac{\partial^2 \Psi}{\partial I_2^2}\right)(\mathbf{I} \otimes \mathbf{C} + \mathbf{C} \otimes \mathbf{I}) + \\
& + \ 4\left(I_3 \frac{\partial^2 \Psi}{\partial I_1 \partial I_3} + I_1 I_3 \frac{\partial^2 \Psi}{\partial I_2 \partial I_3}\right)(\mathbf{I} \otimes \mathbf{C}^{-1} + \mathbf{C}^{-1} \otimes \mathbf{I}) + 4\frac{\partial^2 \Psi}{\partial I_2^2}\mathbf{C} \otimes \mathbf{C} + \\
& - \ 4I_3 \frac{\partial^2 \Psi}{\partial I_2 \partial I_3}(\mathbf{C} \otimes \mathbf{C}^{-1} + \mathbf{C}^{-1} \otimes \mathbf{C}) + 4\left(I_3 \frac{\partial \Psi}{\partial I_3} + I_3^2 \frac{\partial^2 \Psi}{\partial I_3^2}\right)\mathbf{C}^{-1} \otimes \mathbf{C}^{-1} + \\
& - \ 4I_3 \frac{\partial \Psi}{\partial I_3}\mathbf{C}^{-1} \odot \mathbf{C}^{-1} - 4\frac{\partial \Psi}{\partial I_2}\mathcal{S} + 4\left(\frac{\partial^2 \Psi}{\partial I_1 \partial I_4} + I_1 \frac{\partial^2 \Psi}{\partial I_2 \partial I_4}\right)(\mathbf{I} \otimes \mathbf{a_0} \otimes \mathbf{a_0} + \mathbf{a_0} \otimes \mathbf{a_0} \otimes \mathbf{I}) + \\
& - \ 4\frac{\partial^2 \Psi}{\partial I_2 \partial I_4}(\mathbf{C} \otimes \mathbf{a_0} + \mathbf{a_0} \otimes \mathbf{a_0} \otimes \mathbf{C}) + 4\frac{\partial^2 \Psi}{\partial I_4^2}\mathbf{a_0} \otimes \mathbf{a_0} \otimes \mathbf{a_0} \otimes \mathbf{a_0} + \\
& + \ 4\left(\frac{\partial^2 \Psi}{\partial I_1 \partial I_5} + I_1 \frac{\partial^2 \Psi}{\partial I_2 \partial I_5}\right)\left(\mathbf{I} \otimes \frac{\partial I_5}{\partial \mathbf{C}} + \frac{\partial I_5}{\partial \mathbf{C}} \otimes \mathbf{I}\right) - 4\frac{\partial^2 \Psi}{\partial I_2 \partial I_5}\left(\mathbf{C} \otimes \frac{\partial I_5}{\partial \mathbf{C}} + \frac{\partial I_5}{\partial \mathbf{C}} \otimes \mathbf{C}\right) + \\
& + \ 4\frac{\partial^2 \Psi}{\partial I_5^2}\left(\frac{\partial I_5}{\partial \mathbf{C}} \otimes \frac{\partial I_5}{\partial \mathbf{C}}\right) + 4\frac{\partial^2 \Psi}{\partial I_4 \partial I_5}\left(\mathbf{a_0} \otimes \mathbf{a_0} \otimes \frac{\partial I_5}{\partial \mathbf{C}} + \frac{\partial I_5}{\partial \mathbf{C}} \otimes \mathbf{a_0} \otimes \mathbf{a_0}\right) + \\
& + \ 4\frac{\partial \Psi}{\partial I_5}\frac{\partial^2 \Psi}{\partial \mathbf{C}\partial \mathbf{C}} + 4I_3 \frac{\partial^2 \Psi}{\partial I_3 \partial I_4}(\mathbf{a_0} \otimes \mathbf{a_0} \otimes \mathbf{C}^{-1} + \mathbf{C}^{-1} \otimes \mathbf{a_0} \otimes \mathbf{a_0}) + \\
& + \ 4I_3 \frac{\partial^2 \Psi}{\partial I_3 \partial I_5}(\mathbf{a_0} \otimes \mathbf{C}\mathbf{a_0} \otimes \mathbf{C}^{-1} + \mathbf{a_0}\mathbf{C} \otimes \mathbf{a_0} \otimes \mathbf{C}^{-1} + \mathbf{C}^{-1} \otimes \mathbf{a_0} \otimes \mathbf{C}\mathbf{a_0} + \mathbf{C}^{-1} \otimes \mathbf{a_0}\mathbf{C} \otimes \mathbf{a_0})
\end{aligned}
\tag{20}
$$

The full expressions of the terms $\mathbf{C}^{-1} \odot \mathbf{C}^{-1}$ and the fourth-order tensor $\mathcal{S} = (\mathbb{I} + \bar{\mathbb{I}})/2$ can be easily found in reference textbooks.

## 3 Higher-order beam and plate CUF finite element

The Unified Formulation for isotropic hyperelastic materials has been already presented by Pagani et al. [22], in which the formulation of hyperelastic beam finite elements in CUF (Carrera Unified Formulation) framework is established. Lately, Augello *et al.* [23] presented the 2D-CUF plate models analyzing different benchmark problems in nearly-incompressible hyperelasticity. In this work, both refined beam (1D) models and plate (2D) models defined in the CUF framework are employed to study fiber-reinforced soft materials structures.

In general, the three-dimensional displacement field is expressed as a polynomial expansion of the *generalized* nodal displacements, coupling approximation expansion theories along the plate thickness or beam cross-section with kinematic models along the mid-surface or beam axis. This expansion technique allows the implementation of higher-order modes, exploited by means of a recursive index notation. In the classical orthonormal $\{x, y, z\}$ Cartesian reference frame, the three-dimensional displacement field for a beam and plate model is then expressed as

$$\text{Beam 1D models:} \quad \mathbf{u}(x, y, z) = F_\tau(x, z)\mathbf{u}_\tau(y) \quad \tau = 1, ..., M \tag{21}$$

$$\text{Plate 2D models:} \quad \mathbf{u}(x, y, z) = F_\tau(z)\mathbf{u}_\tau(x, y) \quad \tau = 1, ..., M \tag{22}$$

where $M$ is the dimension of the polynomial expansion basis, related to the polynomial order expansion theory along the plate thickness or beam cross-section, and $F_\tau$ are the theory expansion functions that characterize the CUF model adopted, and finally $\mathbf{u}_\tau$ is the vector of generalized displacement components along the reference direction.



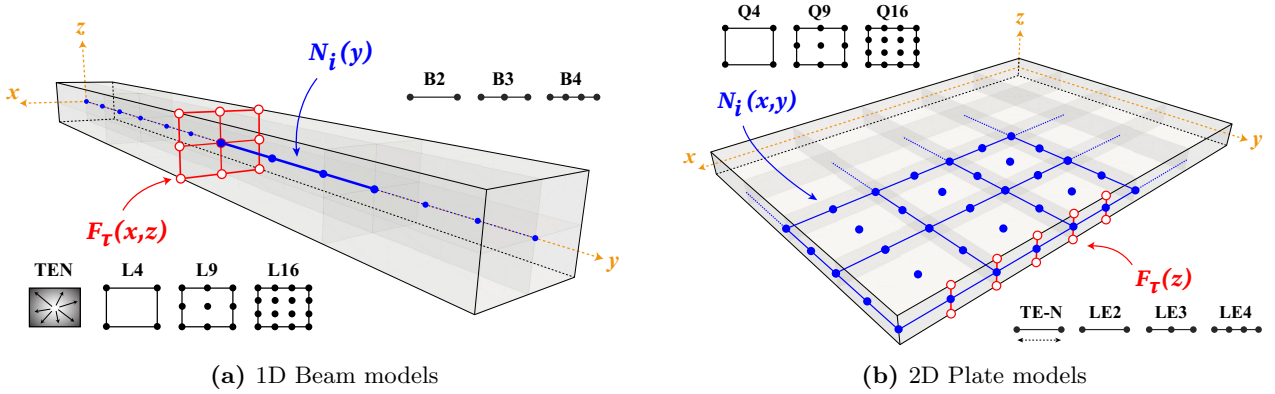**(a)** 1D Beam models      **(b)** 2D Plate models

**Figure 2:** High order 1D and 2D CUF models.

Einstein's notation for repeated indices summation is considered in the definition of the displacement field in Eq. (22). This enables the implementation of higher-order structural theories by selecting the expansion basis function $F_\tau(x, z)$, which fully describes the model. In the present work, two distinct sets of expansion functions are considered for the cross-section expansion or thickness expansion the TE (Taylor Expansion) class and the LE (Lagrange Expansion) class. TE models utilize 1D or 2D MacLaurin polynomials, depending on the model, as basis functions for expanding the generalized reference displacement field (beam axis displacements or mid-surface plate displacements). Based on the chosen expansion order, higher-order theories are automatically defined in a hierarchical manner. As examples, we present the TE-1 linear expansion model, either for the 1D or 2D CUF models, which are

$$\text{1D:} \begin{cases} u_x(x, y, z) = u_{x_1}(y) + x u_{x_2}(y) + z u_{x_3}(y) \\ u_y(x, y, z) = u_{y_1}(y) + x u_{y_2}(y) + z u_{y_3}(y) \\ u_z(x, y, z) = u_{z_1}(y) + x u_{z_2}(y) + z u_{z_3}(y) \end{cases} \quad \text{2D:} \begin{cases} u_x(x, y, z) = u_{x_0}(x, y) + u_{x_1}(x, y) \\ u_y(x, y, z) = u_{y_0}(x, y) + u_{y_1}(x, y) \\ u_z(x, y, z) = u_{z_0}(x, y) + u_{z_1}(x, y) \end{cases} \tag{23}$$

where $u_{x_i}$, $u_{y_i}$ and $u_{z_i}$, in each definition, is the *generalized* displacement variable, unknown of the

problem, by which the whole three-dimensional displacement field is reconstructed by the expansion on $F_\tau$ expansion functions.



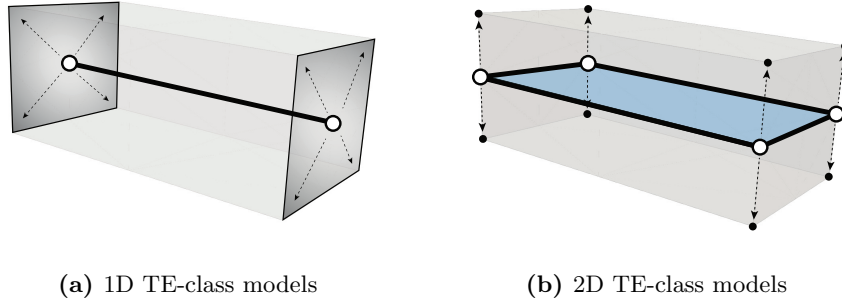**(a)** 1D TE-class models          **(b)** 2D TE-class models

**Figure 3:** TE-class models, graphical representation of the mathematical model.

The TE-class models are generally referred to as ESLMs (Equivalent Single Layer Models), in which the displacement field of the structures is seen as an *homogenized* quantity combining each cross-section sub-components or a single layer of multilayered plates/shells in an equivalent but unique representative structure, taking into account the features of each sub-components.

In the case of LE-models instead, cross-section or thickness elements are defined starting from the set of Lagrange's polynomials adopted and the total number of finite nodes involved. The resulting model, in both cases, is a pure displacement-based model along the cross-section or thickness of the beam, by exploiting the isoparametric formulation. In the present work, linear, parabolic, and cubic expansion models will be adopted. From now on, 1D-CUF LE expansion models will be referred to as four-node linear L4, nine-node parabolic L9, and quadratic six-node cubic L16 cross-section expansion models, instead 2D-CUF expansion models will be addressed as linear LE2, parabolic LE3, and cubic LE4. As examples, we report the displacement field of a 1D-L9 and 2D-LE2 parabolic expansion model, expressed as
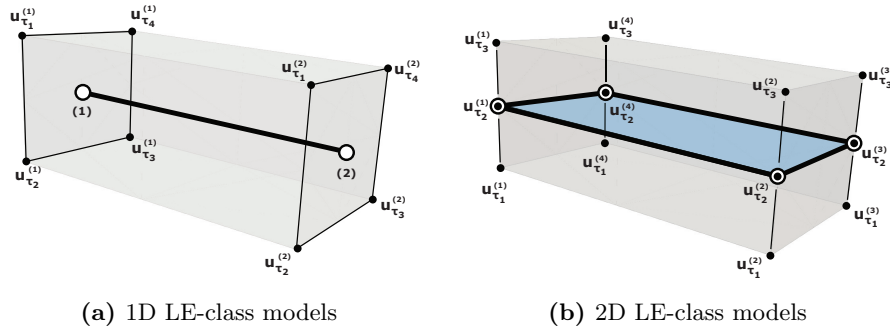


**(a)** 1D LE-class models          **(b)** 2D LE-class models

**Figure 4:** LE-class models, graphical representation of the mathematical model.

$$\text{1D:} \begin{cases} u_x(x,y,z) = F_1(x,z)u_{x_1}(y) + F_2(x,z)u_{x_2}(y) + F_3(x,z)u_{x_3} + \ ... \ + F_9(x,z)u_{x_9}(y) \\ u_y(x,y,z) = F_1(x,z)u_{y_1}(y) + F_2(x,z)u_{y_2}(y) + F_3(x,z)u_{y_3} + \ ... \ + F_9(x,z)u_{y_9}(y) \\ u_z(x,y,z) = F_1(x,z)u_{z_1}(y) + F_2(x,z)u_{z_2}(y) + F_3(x,z)u_{z_3} + \ ... \ + F_9(x,z)u_{z_9}(y) \end{cases} \quad (24)$$

$$\text{2D:} \begin{cases} u_x(x,y,z) = F_1(z)u_{x_1}(x,y) + F_2(z)u_{x_2}(x,y) + F_3(z)u_{x_3}(x,y) \\ u_y(x,y,z) = F_1(z)u_{y_1}(x,y) + F_2(z)u_{y_2}(x,y) + F_3(z)u_{y_3}(x,y) \\ u_z(x,y,z) = F_1(z)u_{z_1}(x,y) + F_2(z)u_{z_2}(x,y) + F_3(z)u_{z_3}(x,y) \end{cases} \quad (25)$$

where the polynomial expansion basis considered is the set of 1D and 2D Lagrange parabolic polynomials. One key feature of LE expansion models is the independent local modeling of cross-section sub-components or multilayered plates/shells, by imposing displacements continuity of purely displacement components. A more detailed derivation of LE-class models and basis function adopted can be found in [26]. The capabilities of higher-order TE expansion models and LE models to deal with component-wise modeling of mechanical and aeronautical structures, the nonlinear static analysis, and pre-stressed vibration analysis are demonstrated in [27, 28, 29].

Independently of the expansion model adopted in the definition of a refined theory, the generalized displacement field components of the 1D CUF beam axis domain or 2D plate mid-surface domain are further discretized by adopting the classical FE approach

$$\text{Beam 1D models:} \qquad \mathbf{u}_\tau(y) = N_i(y)\mathbf{u}_{\tau i} \quad i = 1, ..., N_n \tag{26}$$

$$\text{Plate 2D models:} \quad \mathbf{u}_\tau(x, y) = N_i(x, y)\mathbf{u}_{\tau i} \quad i = 1, ..., N_n \tag{27}$$

where the beam axis or plate mid-surface displacement components are formulated as a general linear combination adopting the $N_i$ shape functions of the discrete nodal displacements $\mathbf{u}_{\tau i}$, unknowns of the model. In Eq. (27), the index $i$ refers to the summation along the finite nodes per element adopted in the discretization of 1D beam axis or 2D plate mid-surface, and $N_n$ refers to the expansion order governed by the total number of finite nodes involved. The final expression of the 3-D displacement field in the CUF domain is then a coupled expansion of structural theories, modeled with the expansion functions, and finite element approximation,

$$\text{Beam 1D models:} \quad \mathbf{u}(x, y, z) = F_\tau(x, z)\mathbf{u}_\tau(y) = F_\tau(x, z)N_i(y)\mathbf{u}_{\tau i} \tag{28}$$

$$\text{Plate 2D models:} \quad \mathbf{u}(x, y, z) = F_\tau(z)\mathbf{u}_\tau(x, y) = F_\tau(z)N_i(x, y)\mathbf{u}_{\tau i} \tag{29}$$

In our proposed model, the finite element approximation of the beam axis will be addressed as linear B2, parabolic B3, and cubic B4 finite elements, instead, the finite element approximation along the plate mid-surface will be referred to as linear Q4, parabolic Q9 and cubic Q16, indicating the total number of finite nodes adopted in the single element definition. Equation (29) is the most general expression of displacement field that immediately the definition of higher-order and refined finite element models for beam and plate structures in a hierarchical manner since it is independent of the polynomial basis adopted in the kinematics of the beam axis or plate mid surface and expansion theories considered.

The difference between these models from a finite element and assembling procedures point of view are shown in Fig. 5. The finite element matrices are combined differently depending on the expansion model chosen, by imposing the superposition of mechanical and stiffness properties in the TE-class case or imposing displacement continuity at interfaces in the LE-class case, in resulting finite element assembling procedures defined straightforwardly.
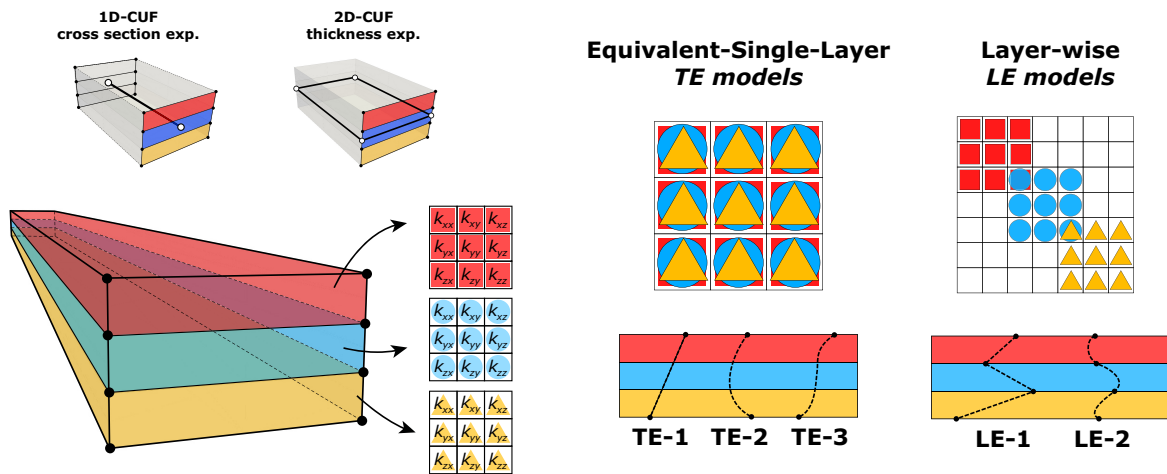


**Figure 5:** Unified models: Equivalent-Single-Layer and Layer-Wise models.

# 4 Nonlinear governing equations in matrix form

## 4.1 Internal and external force vector

In this work, governing equation in weak form are derived by means of the PVD (Principle of Virtual Displacements). Considering a static nonlinear problem, supposing negligible body forces, PVD states

$$\delta\mathcal{L}_{int} = \delta\mathcal{L}_{ext} \tag{30}$$

where $\mathcal{L}_{int}$ is the internal work, $\mathcal{L}_{ext}$ is the external work and $\delta$ denotes the virtual variation. Analytically, these terms can be expressed as

$$\text{(a) } \delta\mathcal{L}_{int} = \int_\Omega \delta\boldsymbol{E}^T \boldsymbol{S} dV \qquad \text{(b) } \delta\mathcal{L}_{ext} = \int_\Omega \delta\boldsymbol{u}^T \mathbf{f} dV \tag{31}$$

where $\mathbf{S}$ is the PK2 stress tensor, $\mathbf{E}$ is the Green-Lagrange strain tensor and $\mathbf{f}$ is the vector of external loads applied. The virtual quantities are introduced adopting the same index notation and polynomial expansion but with independent indices, adopting the $j$ index for virtual measures along the axis nodes and the $s$ index for the CUF expansion model, to obtain independent quantities with respect to real ones. Since both 1D beam models and 2D plate models are considered, variable dependency will be neglected from now on without loss of generality, since the derivation procedure is independent of the model adopted. The generic virtual displacement is then defined as

$$\delta\mathbf{u}(x,y,z) = F_s\mathbf{u}_s = F_s N_j \delta\mathbf{u}_{sj} \qquad j = 1, 2, .., N_n, \quad s = 1, ..., M \tag{32}$$

Referring to the internal energy contribution, the full Green-Lagrange strain tensor can be rewritten in terms of nodal displacement unknowns and expansion functions with the same index notation. Introducing now *Voigt's notation* for the representation of physical symmetric quantities, stress, and deformation tensors are rewritten in vector form as

$$\boldsymbol{S} = \{S_{xx}, S_{yy}, S_{zz}, S_{xz}, S_{yz}, S_{xy}\}^T \tag{33}$$

$$\boldsymbol{E} = \{E_{xx}, E_{yy}, E_{zz}, E_{xz}, E_{yz}, E_{xy}\}^T \tag{34}$$

Under the hypothesis of the fully nonlinear displacement-strain relation, the Green-Lagrange tensor can be rewritten as done in Pagani *et al.* [19]

$$\boldsymbol{E} = (\mathbf{b_l} + \mathbf{b_{nl}})\,\mathbf{u} = (\mathbf{b_l} + \mathbf{b_{nl}})\,F_\tau N_i \mathbf{u}_{\tau i} = (\mathbf{B_l}^{\tau i} + \mathbf{B_{nl}}^{\tau i})\mathbf{u}_{\tau i} \tag{35}$$

Applying the formal matrices of derivatives operator $\mathbf{b_l}$ and $\mathbf{b_{nl}}$ to CUF expansion of the displacement field, the algebraic matrices $\mathbf{B_l}^{\tau i}$ and $\mathbf{B_{nl}}^{\tau i}$ are obtained, and their explicit forms can be found in [19, 20]. The virtual variation of the strain measure is written in compact form including the previously introduced discretization of virtual displacement Eq.(32)

$$\delta\boldsymbol{E} = \delta((\mathbf{B_l}^{\tau i} + \mathbf{B_{nl}}^{\tau i})\mathbf{u}_{\tau i}) = (\mathbf{B_l}^{sj} + 2\mathbf{B_{nl}}^{sj})\delta\mathbf{u}_{sj} \tag{36}$$

Substituting now Eq.(36) into Eq.(31)(a)

$$\delta\mathcal{L}_{int} = \int_\Omega \delta\mathbf{u}_{sj}^T (\mathbf{B_l}^{sj} + 2\mathbf{B_{nl}}^{sj})^T \boldsymbol{S} dV = \delta\mathbf{u}_{sj}^T \mathbf{F}_{int}^{sj} \tag{37}$$

where $\mathbf{F}_{int}^{sj}$ the 3x1 FN (Fundamental Nucleus) of the internal forces vector

$$\mathbf{F}_{int}^{sj} = \int_\Omega (\mathbf{B_l}^{sj} + 2\mathbf{B_{nl}}^{sj})^T \boldsymbol{S} dV \tag{38}$$

Referring to the external load contribution in the variational principle, the FN of the external load vector is exploited by means of the same derivation procedure described for the internal energy contribution. If $\mathbf{f}$ is the vector of conservative loads applied to the structure, one has

$$\delta\mathcal{L}_{ext} = \int_\Omega \delta\boldsymbol{u}^T \mathbf{f} dV = \int_\Omega \delta\mathbf{u}_{sj}^T F_s N_j \mathbf{f}\,dV = \delta\mathbf{u}_{sj}^T \mathbf{F}_{ext}^{sj} \tag{39}$$

where $\mathbf{F}_{ext}^{sj}$ the 3x1 FN of the external forces vector

$$\mathbf{F}_{ext}^{sj} = \int_\Omega F_s N_j \mathbf{f}\ dV \tag{40}$$

The main advantage in the adoption of CUF-based finite element models is herein noticeable by Eq.(38) and Eq.(39) the FNs of physical quantities are defined regardless of the specific kinematic model adopted in the discretization of finite nodes and approximation theory along the cross-section or thickness of the structure, therefore independent expressions of physical quantities for any arbitrarily polynomial expansion are found. The unique expressions of internal forces and external forces for specific combinations of models adopted are exploited by assigning the finite element shape functions $N_i$, $N_j$ and theory of structure approximation $F_\tau$ and $F_s$ of any order, and exploiting the summation over the recursive indices expansion (namely the summation over indices i and j, $\tau$, and s). Finally, the PVD is written in compact notation as follow

$$\delta\mathbf{u}_{sj}: \quad \mathbf{F}_{int}^{sj} - \mathbf{F}_{ext}^{sj} = 0 \tag{41}$$

Considering the summation over indices $s$ and $j$, the global internal forces vector $\mathbf{F}_{int}$ and external load vector $\mathbf{F}_{int}$ can be computed, following the CUF assembling procedure [15].

In a finite element scenario for hyperelasticity, both large displacements and rotations (geometrical nonlinearities) and nonlinear constitutive law (material nonlinearities) must be taken into account for these reasons, equilibrium equations turn out to be strongly nonlinear, and common solution techniques are based on numerical iterative solvers.

## 4.2 Linearization of governing equations

The expanded nonlinear problem Eq.(41) is written as an equivalent optimization problem in the form of minimization of residual function [30]. Defining the *unbalanced nodal forces vector* as

$$\phi_{\mathbf{res}} = \mathbf{F}_{int} - \mathbf{F}_{ext} \tag{42}$$

the solution of the nonlinear equilibrium problem is equivalent to finding the root of Eq.42 since, at equilibrium, due to balance the residual nodal forces vector is null ($\phi_{\mathbf{res}} = 0$). In our formulation, a Newton-Raphson iterative scheme is employed, thus expanding Eq.(42) by considering Taylor's expansion around a known condition $(\mathbf{u^0}, \mathbf{F}_{ext}^0)$ truncated at the first order

$$\phi_{\mathbf{res}}(\mathbf{u}^0 + \Delta\mathbf{u}, \mathbf{F}_{ext} + \Delta\mathbf{F}_{ext}) = \phi_{\mathbf{res}}(\mathbf{u}^0, \mathbf{F}_{ext}^0) + \frac{\partial\phi_{\mathbf{res}}}{\partial\mathbf{u}}\Delta\mathbf{u} + \frac{\partial\phi_{\mathbf{res}}}{\partial\mathbf{F}_{ext}}\Delta\lambda \cdot \mathbf{F}_{ext}^{rif} = 0 \tag{43}$$

where the finite variation of the nodal load vector can be rearranged under the hypothesis of conservative external load, in mathematical terms $\Delta\mathbf{F}_{ext} = \Delta(\lambda\mathbf{F}_{ext}^{ref}) = \Delta\lambda\mathbf{F}_{ext}^{ref}$. Defining the tangent stiffness matrix as $\frac{\partial\phi_{\mathbf{res}}}{\partial\mathbf{u}} = \mathbf{K}_T$ and recognizing that $\frac{\partial\phi_{\mathbf{res}}}{\partial\mathbf{F}_{ext}} = -\mathbf{I}$, Eq.(43) is written as

$$\mathbf{K}_T(\mathbf{u}^0)\Delta\mathbf{u} = \Delta\lambda\mathbf{F}_{ext}^{ref} - \phi_{\mathbf{res}}(\mathbf{u}^0, \mathbf{F}_{ext}^0) \tag{44}$$

Considering the *loading scale parameter* $\lambda$ as an additional variable of the problem, Eq.(44) must be coupled with a general constraint equation, to close algebraically the problem, thus

$$\begin{cases} \mathbf{K}_T(\mathbf{u}^0)\Delta\mathbf{u} = \Delta\lambda\mathbf{F}_{ext}^{ref} - \phi_{\mathbf{res}}(\mathbf{u}^0, \mathbf{F}_{ext}^0) \\ c(\Delta\mathbf{u}, \Delta\lambda) = 0 \end{cases} \tag{45}$$

The constraint equation characterizes the numerical scheme adopted, one can implement displacement control, load control, and path-following methods by adopting a different constraint. In the present work, the path-following method proposed by Crisfield [31] is employed, and the implementation of such arc-length iterative solver in a CUF-based finite element scenario is described in detail in [19].

### 4.3 Tangent stiffness matrix

The analytic expression of the tangent stiffness matrix is here described in detail and exploited by linearization of equilibrium equation Eq.(42). Through the assumption of conservative loads only the virtual variation of the internal work has to be linearized, since the second variation of external loads will be identically null, therefore the finite variation of the internal strain energy contribution of the variational principle is

$$\Delta(\delta\mathcal{L}_{int}) = \int_{\Omega} \Delta(\delta\boldsymbol{E}^T\boldsymbol{S})dV = \int_{\Omega} \delta\boldsymbol{E}^T\Delta\boldsymbol{S}dV + \int_{\Omega} \Delta(\delta\boldsymbol{E}^T)\boldsymbol{S}dV \tag{46}$$

The two integral terms appearing in Eq.(46) are now analyzed separately.

The first term represent the linearization of constitutive equation. Adopting Holzapfel formulation, Eq.(18) is rewritten in matrix form

$$\Delta\mathbf{S} = \mathbb{C}\frac{1}{2}\Delta\mathbf{C} = \mathbb{C}\Delta\mathbf{E} = \mathbb{C}(\mathbf{B_l}^{sj} + 2\mathbf{B_{nl}}^{sj})\Delta\mathbf{u}_{sj} \tag{47}$$

Thus, the linearization of the constitutive equation can be written as

$$\begin{aligned}
\int_{\Omega} \delta\boldsymbol{E}^T\Delta\boldsymbol{S}dV &= \int_{\Omega} \delta\mathbf{u}_{sj}^T(\mathbf{B_l}^{sj} + 2\mathbf{B_{nl}}^{sj})^T\mathbb{C}(\mathbf{B_l}^{\tau i} + \mathbf{B_{nl}}^{\tau i})\Delta\mathbf{u}_{\tau i} \ dV = \\
&= \delta\mathbf{u}_{sj}^T\mathbf{K}_{ll}^{\tau sij}\Delta\mathbf{u}_{\tau i} + \delta\mathbf{u}_{sj}^T\mathbf{K}_{lnl}^{\tau sij}\Delta\mathbf{u}_{\tau i} + \delta\mathbf{u}_{sj}^T\mathbf{K}_{nll}^{\tau sij}\Delta\mathbf{u}_{\tau i} + \delta\mathbf{u}_{sj}^T\mathbf{K}_{nlnl}^{\tau sij}\Delta\mathbf{u}_{\tau i} = \\
&= \delta\mathbf{u}_{sj}^T\mathbf{K}_{ll}^{\tau sij}\Delta\mathbf{u}_{\tau i} + \delta\mathbf{u}_{sj}^T\mathbf{K}_{T_1}^{\tau sij}\Delta\mathbf{u}_{\tau i}
\end{aligned} \tag{48}$$

where $\mathbf{K}_{T_1}^{\tau sij} = \mathbf{K}_{lnl}^{\tau sij} + \mathbf{K}_{nll}^{\tau sij} + \mathbf{K}_{nlnl}^{\tau sij}$ is the non linear contribution to the tangent stiffness matrix coming from the linearization of the constitutive equation and $\mathbf{K}_{ll}^{\tau sij}$ is the linear contribution.

The second term of Eq.(46) is the linearization of geometrical relations. Exploiting the same derivation procedure described before, one can find the fundamental nucleus of the *geometrical* stiffness matrix $\mathbf{K}_{\sigma}^{\tau sij}$, the derivation will be not reported here but can be found explicitly in [19, 20].

$$\int_{\Omega} \Delta(\delta\boldsymbol{E})^T\boldsymbol{S}dV = \delta\mathbf{u}_{sj}^T\mathbf{K}_{\sigma}^{\tau sij}\Delta\mathbf{u}_{\tau i} \tag{49}$$

Substituting finally the expression of the contribution coming from the linearization of the constitutive equation Eq.(48) and the one coming from linearization of the geometrical relations Eq.(49), the fundamental nucleus of the tangent stiffness matrix is defined as

$$\begin{aligned}
\Delta(\delta\mathcal{L}_{int}) &= \int_{\Omega} \delta\boldsymbol{E}^T\Delta\boldsymbol{S}dV + \int_{\Omega} \Delta(\delta\boldsymbol{E})^T\boldsymbol{S}dV = \\
&= \delta\mathbf{u}_{sj}^T\mathbf{K}_{ll}^{\tau sij}\Delta\mathbf{u}_{\tau i} + \delta\mathbf{u}_{sj}^T\mathbf{K}_{T_1}^{ij}\Delta\mathbf{u}_{\tau i} + \delta\mathbf{u}_{sj}^T\mathbf{K}_{\sigma}^{\tau sij}\Delta\mathbf{u}_{\tau i} = \\
&= \delta\mathbf{u}_{sj}^T\mathbf{K}_{T}^{\tau sij}\Delta\mathbf{u}_{\tau i}
\end{aligned} \tag{50}$$

As stressed in the previous theoretical derivation of the model, the FNs of sub-matrices of the tangent stiffness matrix are defined for any arbitrary polynomial expansion chosen. The unique expression of tangent stiffness matrix in the single CUF finite element is achieved by exploiting the summation over indices i and j, $\tau$ and s, thus on shape functions $N_i$, $N_i$ and theory of structure approximation $F_\tau$ and $F_s$, but the resulting definition of FN is completely independent of the chosen kinematic models and approximation theory.

# 5 Numerical results

In this section, numerical results obtained via the present implementation of higher-order 1D beam dn 2D plate CUF models for transversely isotropic hyperelastic materials are presented and validated adopting as reference results popular benchmark problems available in literature or simple cases in which closed-form solutions are known. We present different models and we investigate the capabilities of our models when different strain energy functions are considered, more complex geometries are involved, and in particular when different preferential directions of the fibers are chosen, analyzing standard problems involving Cartesian or curvilinear geometries.

## 5.1 Shear test of an incompressible block

The first problem is a simple shear test of a fiber-reinforced incompressible cubic block. This classical benchmark problem in hyperelasticity is a special case for which closed-form solutions are known. Geometry and boundary conditions are depicted in Fig. 6.



**(a)** Geometry and boundary conditions    **(b)** Deformed configuration
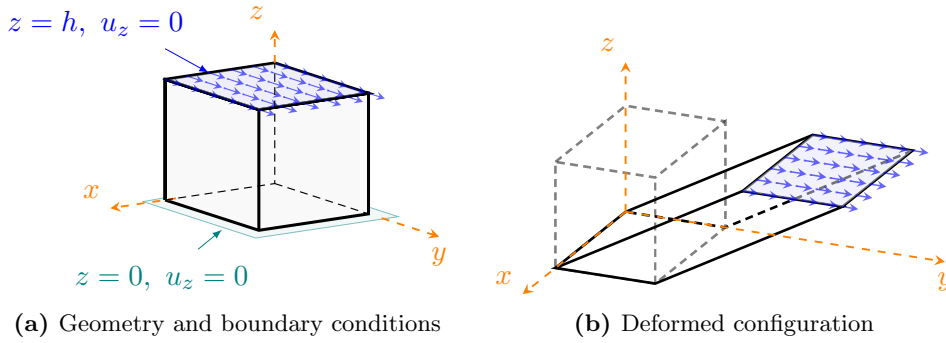
**Figure 6:** Simple shear tension test, description of the problem.

Material is modeled adopting a refined version of the classical HGO (Holzapfel-Gasser-Ogden) model for fiber-reinforced materials [2] and presented in Mendez at al. [32], in which the authors proposed this refined strain energy function to investigate the physical meaning of $I_5$ invariant

$$\Psi = \Psi_{vol}(I_3) + \Psi_{iso}(I_1, I_2, I_3) + \Psi_{ani}(I_3, I_4, I_5) \tag{51}$$

$$\Psi_{vol}(I_3) = \frac{k}{2}(J-1)^2 = \frac{k}{2}(\sqrt{I_3}-1)^2 \tag{52}$$

$$\Psi_{iso}(I_1, I_2, I_3) = \frac{c_1}{2}(\bar{I}_1 - 1) = \frac{c_1}{2}(I_1 I_3^{-1/3} - 1) \tag{53}$$

$$
\begin{aligned}
\Psi_{aniso}(I_3, I_4, I_5) &= \frac{c_2}{2c_3}(e^{c_3(\bar{I}_4-1)^2} - 1) + \frac{c_4}{2c_5}(e^{c_5(\bar{I}_5 - \bar{I}_4^2)^2} - 1) = \\
&= \frac{c_2}{2c_3}(e^{C_3(I_4 I_3^{-1/3}-1)^2} - 1) + \frac{c_4}{2c_5}(e^{c_5(I_5 I_3^{-2/3} - I_4^2 I_3^{-2/3})^2} - 1)
\end{aligned} \tag{54}
$$

Material parameters adopted numerical constants considered are described in Table 1.

We now derive the explicit analytic expression of deformation gradient components, thus the analytic expression of the non-null terms of PK2 stress tensor. If $\{x^0, y^0, z^0\}$ are the coordinates of the generic material point of the cube in the reference configuration and $\{x, y, z\}$ are the coordinate in the deformed configuration, as previously shown in Fig. 1, the deformation field components for the shear problem in the $y-z$ plane shown in Fig.6 are known, thus also the deformation gradient and the right Cauchy-Green strain tensor

$$(x, y, z) = f(x^0, y^0, z^0) \begin{cases} x = x^0 \\ y = y^0 + \gamma z^0 \\ z = z^0 \end{cases} \rightarrow \mathbf{F} = \begin{bmatrix} 1 & 0 & 0 \\ 0 & 1 & \gamma \\ 0 & 0 & 1 \end{bmatrix} \rightarrow \mathbf{C} = \mathbf{F}^T \mathbf{F} = \begin{bmatrix} 1 & 0 & 0 \\ 0 & 1 & \gamma \\ 0 & \gamma & 1+\gamma^2 \end{bmatrix}$$

12

where $\gamma$ is a strictly positive real number. Supposing again that $\mathbf{a_0} = (a_x, a_y, a_z)^T$, invariants and pseudo-invariants required for the computation of physical quantities are

$$\begin{cases} I_1 = 3 + \gamma^2 \\ I_2 = -3 - 2\gamma^2 \\ I_3 = 1 \end{cases} \qquad \begin{cases} I_4 = a_x^2 + a_y(a_y + a_z\gamma) + a_z(a_y\gamma + a_z(1 + \gamma^2)) \\ I_5 = a_x^2 + a_y(a_y + a_z\gamma^2) + a_z(a_y\gamma^2 + a_z(1 + \gamma^2)^2) \end{cases}$$

One can note that $J = \det \mathbf{F} = 1$, so the mathematical enforcement of incompressibility is obtained by imposing the deformation gradient components. Computing then the derivatives of strain energy function Eq.(51), and computing the analytic expression of the stress tensor $\mathbf{S}$ by Eq.(17), finally the analytic expression of Cauchy's "true" stress tensor function of the shear parameter $\gamma$ is obtained

$$\boldsymbol{\sigma} = \frac{1}{J}\mathbf{F}\mathbf{S}\mathbf{F}^T \qquad (55)$$

Due to the analytic complexity, here extended expression of PK2 stress components are not reported but they can be computed easily. In this study case, the capabilities of the present implementation of CUF-based models are investigated by analyzing the mechanical behavior when different fiber directions are considered. To validate the present implementation of hyperelastic 1D and 2D CUF models, the cubic specimen is analyzed by two independent models in the first case, the mathematical model adopted makes use of 1D beam elements, with one L4 linear element adopted for the cross-section discretization and one B2 linear element along the axis; in the case of 2D plate CUF models, only one Q4 linear element is adopted in the discretization of the mid-surface and one LE2 linear element is adopted for the thickness expansion theory. In particular, the mechanical response of the cube is analyzed in six different study cases, for each discretization adopted, in which different fiber vectors are considered.

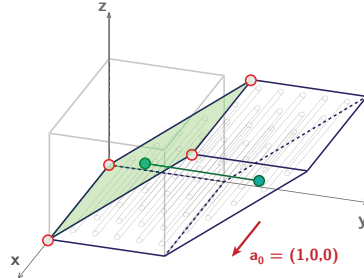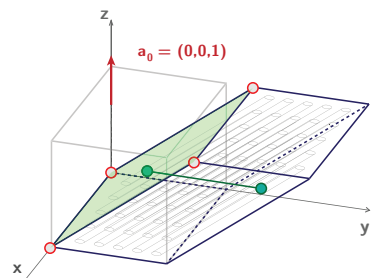| $k$ [kPa] | $c_1$ [kPa] | $c_2$ [kPa] | $c_3$ [ - ] | $c_4$ [kPa] | $c_5$ [ - ] |
|-----------|-------------|-------------|-------------|-------------|-------------|
| $1 \cdot 10^8$ | 50 | 831.4 | 4.241 | 350.96 | 6.18 |

**Table 1:** Simple shear problem material properties

Figure 7(a), Fig. 7(b) and Fig. 7(c) depict, for each unitary versor $\mathbf{a_0}$ considered, the geometrical model of the fiber-reinforcement considered and the 1D CUF finite element adopted, instead Fig. 7(d), Fig. 7(e) and Fig. 7(f) show the comparison between the analytic stress-stretch curve and the numerical results obtained by discretizing the specimen with 1LE2-1B2 beam CUF element, plotting the stress distribution versus the shear parameter $\gamma$ in all cases, a perfect superposition of the numerical results is achieved. The same analysis is performed adopting the indicated 2D plate discretization of the cubic specimen, but for the sake of brevity, results are not reported here since actual numerical results perfectly match the one already presented. As another example, following the proposed study cases in Mendez *et al.* [32], the mechanical response of the cubic specimen is analyzed in the case of a preferential direction of the fibers laying in the $y - z$ plane, inclined of an angle $\theta$ with respect to the y-axis. Three different inclination conditions are proposed $\theta = 30°$, $\theta = 45°$ and $\theta = 60°$. Figure 7(g), Fig. 7(h) and 7(i) shows the comparison between analytic and numeric stress-stretch curves in the case of 1Q4-1B2 results are perfectly matching the analytic solution in all the cases.
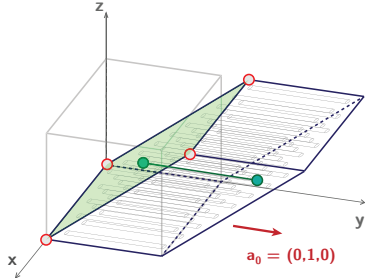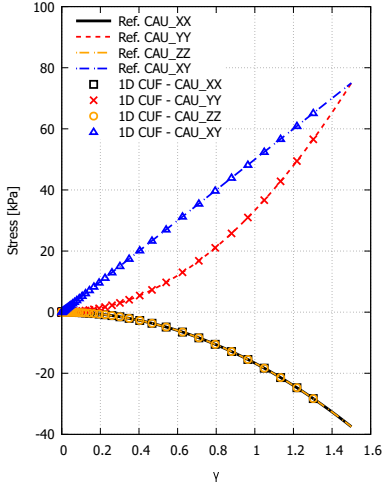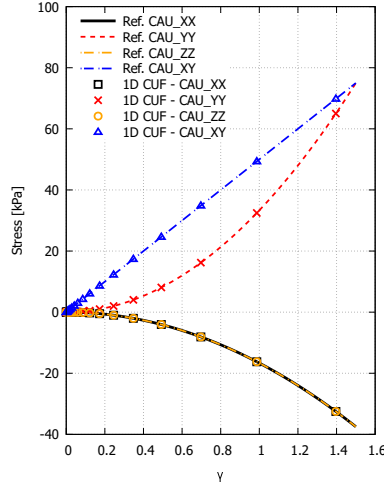
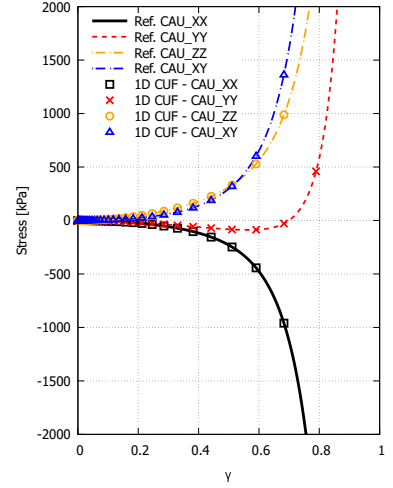**(a)** Configuration $\mathbf{a_0} = (0, 1, 0)$      **(b)** Configuration $\mathbf{a_0} = (1, 0, 0)$      **(c)** Configuration $\mathbf{a_0} = (0, 0, 1)$
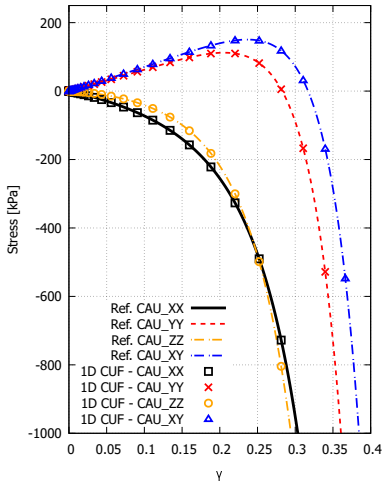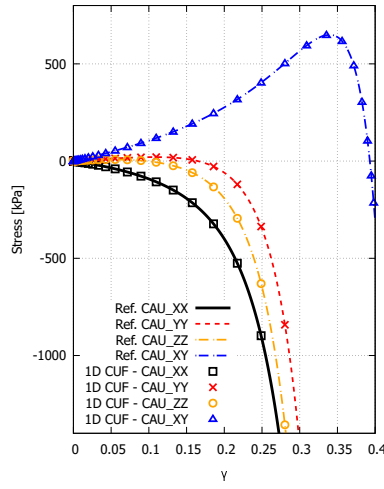
**(d)** $\mathbf{a_0} = (0, 1, 0)$      **(e)** $\mathbf{a_0} = (1, 0, 0)$      **(f)** $\mathbf{a_0} = (0, 0, 1)$
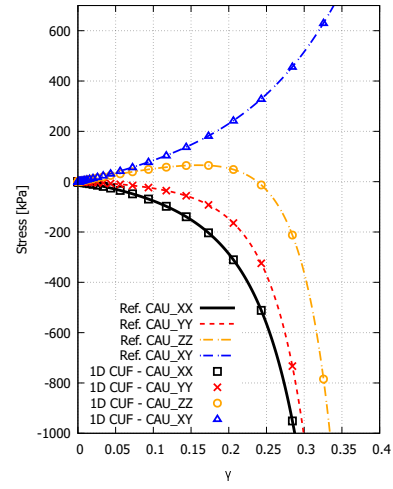
**(g)** $\mathbf{a_0} = (0, \cos 30°, \sin 30°)$      **(h)** $\mathbf{a_0} = (0, \cos 45°, \sin 45°)$      **(i)** $\mathbf{a_0} = (0, \cos 60°, \sin 60°)$

**Figure 7:** Shear tension test comparison between analytic and 1D beam CUF numerical solution

14

## 5.2 Circular plate under uniform transversal pressure

As a second numerical example, the bending of a circular plate presented by Beheshti *et al.* [13] is considered a benchmark case study. A circular plate of radius $R = 50$ mm and thickness $h = 5$ mm clamped at the lateral surface is subjected to a vertical transversal pressure $\mathbf{q}_z$. The geometrical features and boundary conditions are depicted in Fig. 8(a).
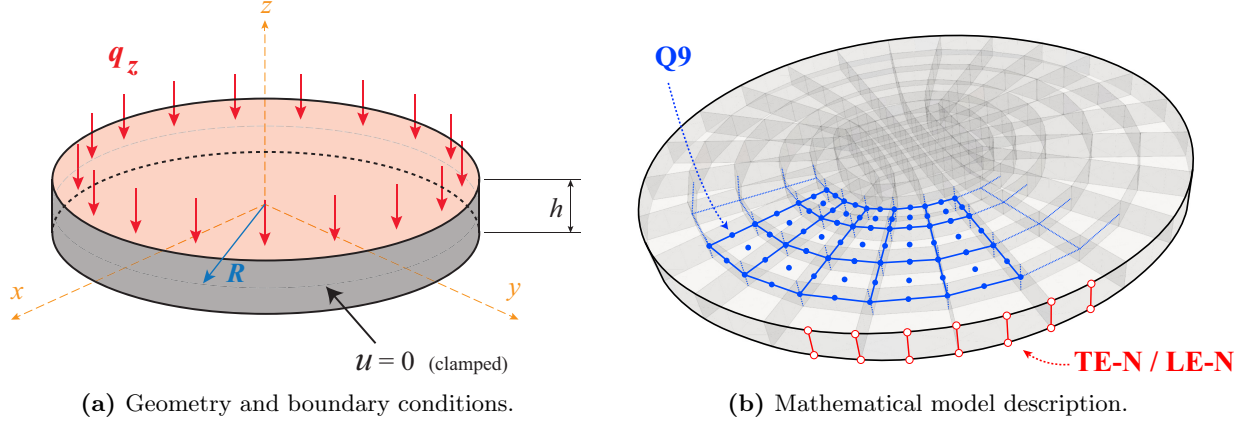


**(a)** Geometry and boundary conditions.

**(b)** Mathematical model description.

**Figure 8:** Circular plate configuration of the case study.

The mechanical response of the plate is investigated for different material conditions in the first case, an isotropic hyperelastic plate is analyzed, and thereafter a fiber-reinforced hyperelastic one in the same geometrical and load conditions. In the anisotropic case, two different fiber distributions are considered separately, a radial reinforcement and then a tangential reinforcement thanks to the numerical integration technique, the unitary vector $\mathbf{a_0}$ required for the computation of physical quantities is defined locally by the Gauss integration point in each element of the discretization.



**(a)** Radial reinforcement.
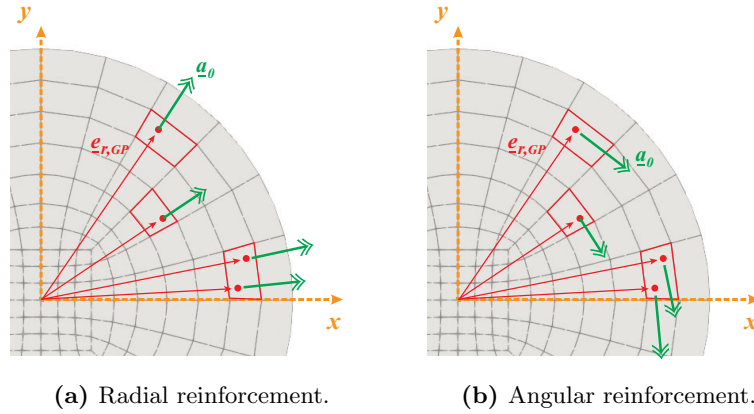
**(b)** Angular reinforcement.

**Figure 9:** Circular plate, anisotropic case, fiber distribution in the definition of principal fiber direction, by taking advantage of the numerical integration scheme employed in stiffness matrices computation, the vector $\mathbf{a_0}$ is defined starting from the physical coordinates of the Gauss integration point, in this way a globally accurate distribution of fibers can be easily obtained.

Material is modeled with an isotropic Neo-Hookean model coupled with the standard reinforcement model for fiber-reinforced hyperelastic material and a stabilized volumetric logarithmic-power model

$$\Psi(\mathbf{C}) = \frac{\mu}{2}(I_1 - 3) + \frac{\lambda}{2}(J - 1)^2 - \mu \log J + \gamma(I_4 - 1)^2 \tag{56}$$

where the infinitesimal shear modulus is set to $\mu = 1$ MPa, the Lame constant is set to $\lambda = 4$ MPa and the reinforcing model constant is $\gamma = 0.375$ MPa. In the case of an isotropic plate, the constant $\gamma$ is set equal to zero.

15

As a preliminary investigation, a convergence analysis is carried out considering 2D plate CUF models, analyzing the influence of different kinematic models adopted in the discretization of plate mid-surface and the influence of the theory approximation along the thickness thus a convergence analysis for an increasing number of Q9 parabolic elements along the mid surface of the plate will be considered, instead the influence of the mathematical model in the expansion along the thickness will be investigated considering linear, quadratic, and cubic Taylor Expansion model and Lagrange Expansion model, that will be addressed as TE$N$ (where N is the polynomial order), LE2 (Lagrange parabolic model) and LE3 (Lagrange cubic model). Actual numerical results obtained adopting 2D plate CUF elements are compared with the reference results, analyzing the structure in the specific configuration of transversely isotropic hyperelastic material with radial fiber distribution.

Figure 10(a) shows the equilibrium paths of the clamped plate in the radial fiber distribution condition analyzing the influence of the total number of finite elements adopted in the discretization on the numerical solution, instead of Fig. 10(b) shows the influence of the mathematical model adopted in the thickness expansion, plotting the vertical transversal displacement of the center of the plate (measured at the mid surface) versus the modulus of applied pressure. In all the cases, a perfect superposition of the numerical results is evidenced, and accurate predictions are obtained.
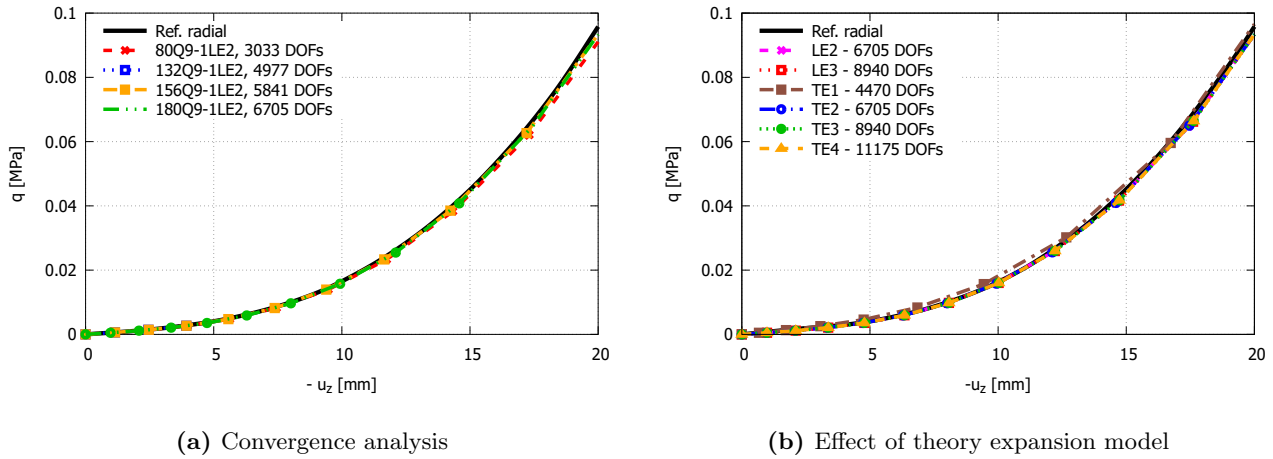


(a) Convergence analysis  (b) Effect of theory expansion model

**Figure 10:** Circular plate equilibrium curve of the plate in the radial fiber distribution configuration.

In the following, the nonlinear static analysis of clamped plate in each described material configuration is carried out the isotropic and fiber-reinforced cases are studied adopting the convergent mathematical model previously described, employing 180 Q9 parabolic elements in the discretization of the plate mid-surface and a single LE3 element along the thickness. Figure 11 shows the equilibrium path for all material configurations, comparing the transversal displacement of the center of the plate (measured on the mid-surface) obtained by 2D CUF models with reference results. Actual numerical solutions are in perfect agreement with the reference solution. In particular, a stiffer behavior of the plate can be observed when a radial distribution of fibers is considered, instead in the case of tangential/angular distribution the mechanical behavior is similar to the isotropic one. In the case of radial fiber distribution, Fig. 12(a) shows the transversal displacement distribution along the plate thickness (measured at the center), instead Fig. 12(b) shows the longitudinal displacement distribution along the diameter of the plate, measured at the mid surface. Again, the linear TE1 model, which corresponds to the first-order shear deformation theory, is not able to capture the correct transversal behavior due to the theoretical model assumptions. Figure 13 shows the deformed configurations of the anisotropic radial reinforced plate in different load conditions.
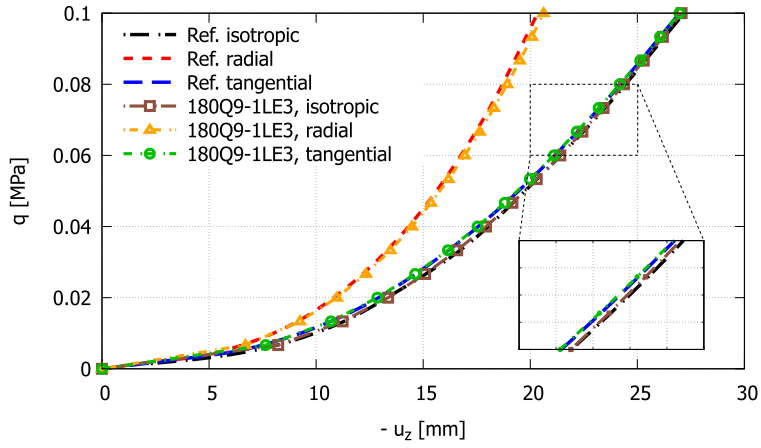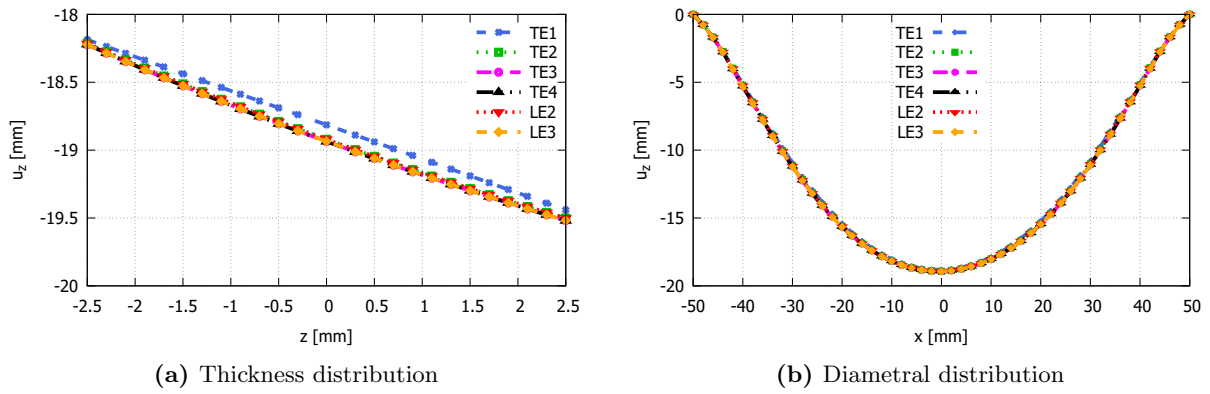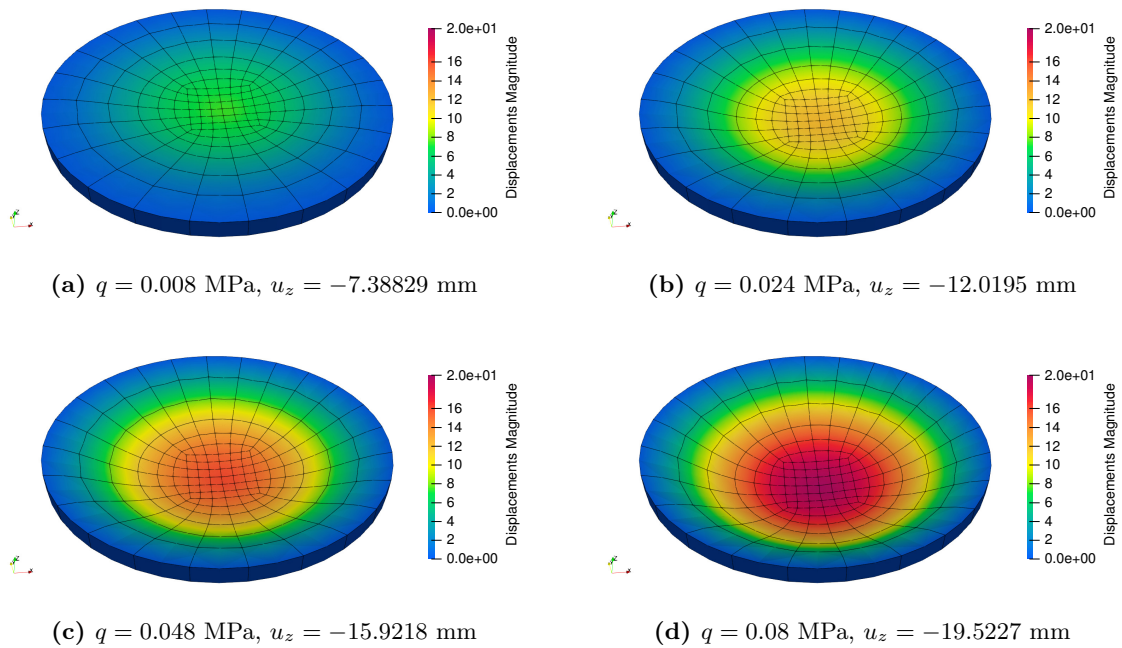
16

**Figure 11:** Circular plate equilibrium path for different fiber configurations.



**(a)** Thickness distribution

**(b)** Diametral distribution

**Figure 12:** Circular plate displacement distribution along the thickness and the diameter of the plate, for various expansion theories, radial fiber distribution case.



**(a)** $q = 0.008$ MPa, $u_z = -7.38829$ mm

**(b)** $q = 0.024$ MPa, $u_z = -12.0195$ mm

**(c)** $q = 0.048$ MPa, $u_z = -15.9218$ mm

**(d)** $q = 0.08$ MPa, $u_z = -19.5227$ mm

**Figure 13:** Circular plate deformed configurations for different value of applied pressure, 180Q9-1LE3

17

Furthermore, the influence of expansion approximation theory on the description of stresses is investigated. The clamped plate is considered now in the isotropic material condition, employing the previously convergent mesh made by 180 Q9 parabolic elements and different expansion models to analyze the through-the-thickness stress distributions. Figure 14 shows the distributions of PK2 stress components along the $z$ direction, measured at the point A positioned at coordinates $(-3/4R, 0)$ mm on the plate mid-surface, when a transversal pressure $q_z = 0.1$ MPa is applied. In all the cases, differences are evidenced between models, which can be addressed to the higher accuracy of the deformation gradient and invariants computation thanks to higher-order expansions of the displacement field, which lead to more accurate predictions of the stress field components.
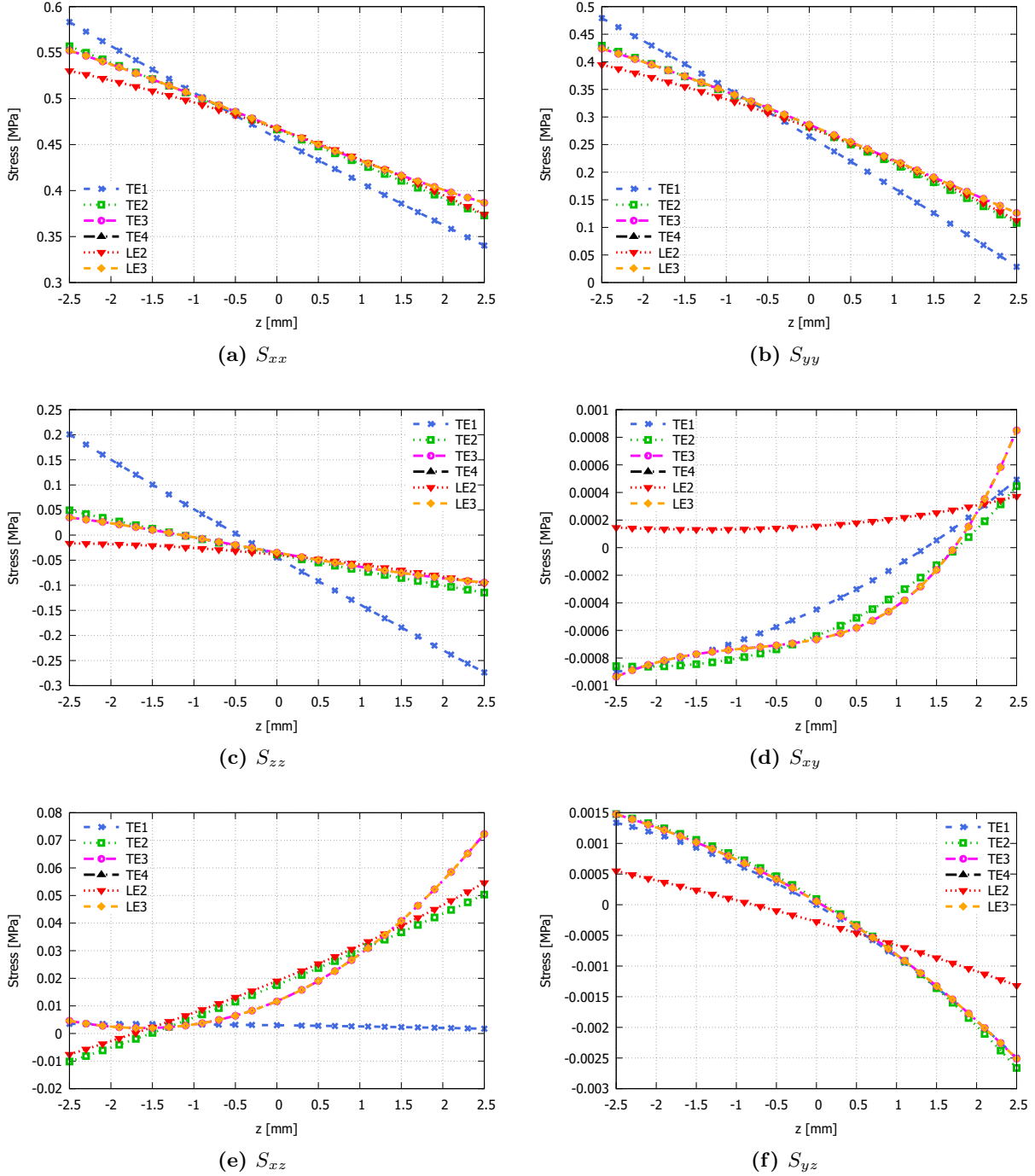


**Figure 14:** Circular plate effects of theory expansion on through-the-thickness stresses distribution, Piola-Kirchoff 2 stresses for the isotropic case and load condition $\mathbf{q}_z = 0.1$ MPa.

18

The same comparison is considered to investigate Cauchy's stress, measured again at the same point and considering the same load configuration. Cauchy's stresses are computed thanks to the deformation gradient and the already available PK2 by Eq. (55). The through-the-thickness distribution of Cauchy's stresses obtained adopting the same expansion approximation theories is shown in Fig. 14. Again, the same considerations previously made are experienced in this last comparison.
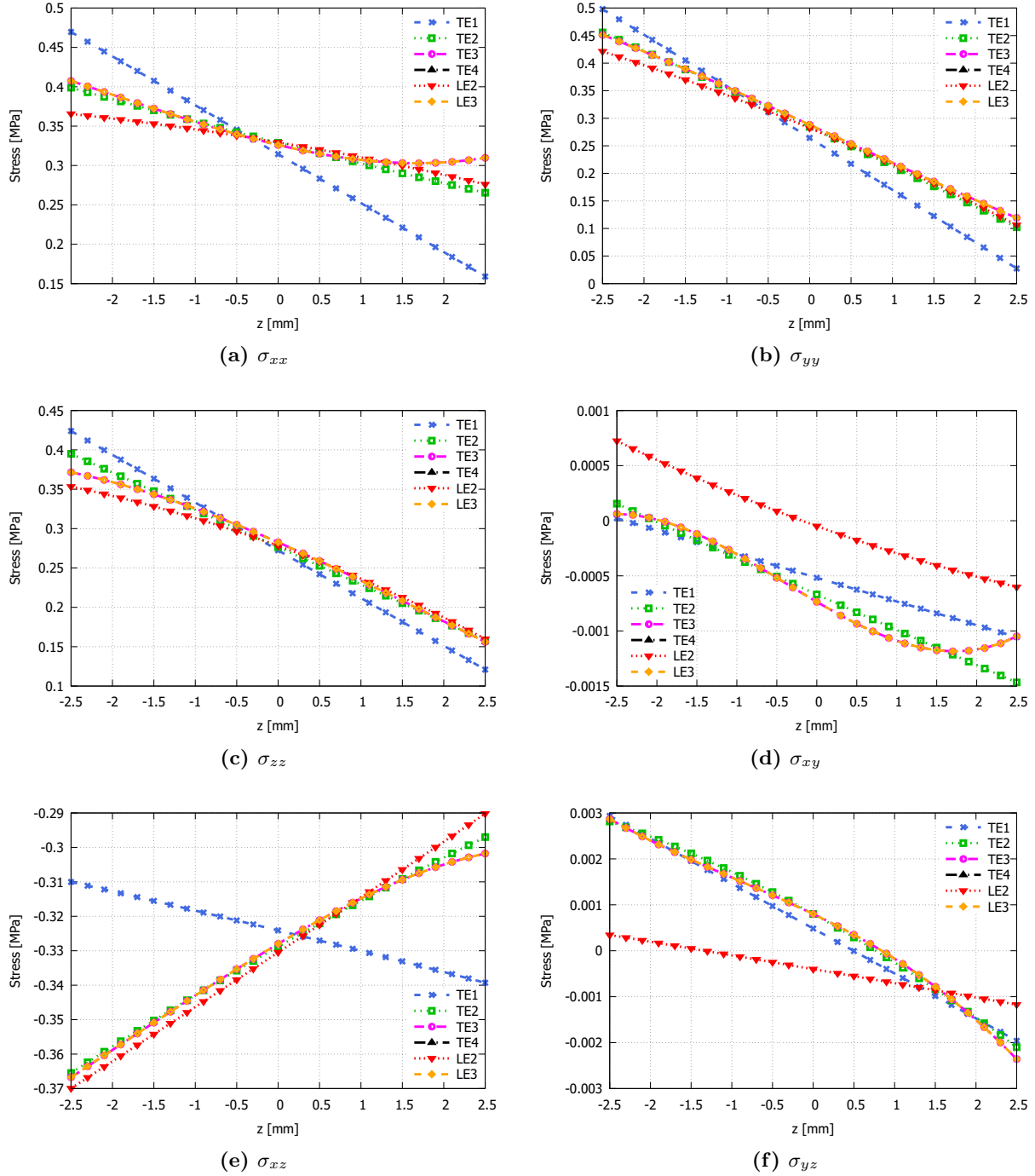


**Figure 15:** Circular plate effects of theory expansion on through-the-thickness stresses distribution, Cauchy's stresses for the isotropic case and load condition $\mathbf{q}_z = 0.1$ MPa.

## 5.3 Cantilever square plate under traction pressure

In this third case study, the large strains analysis of a cantilever square plate, presented by Beheshti *et al.* [13], is carried out. A square plate of lateral length $a = 20$ mm and thickness $t = 1$ mm is subjected to a tensile pressure load at the free end of the plate. The geometrical features and boundary conditions are depicted in Fig. 16(a).



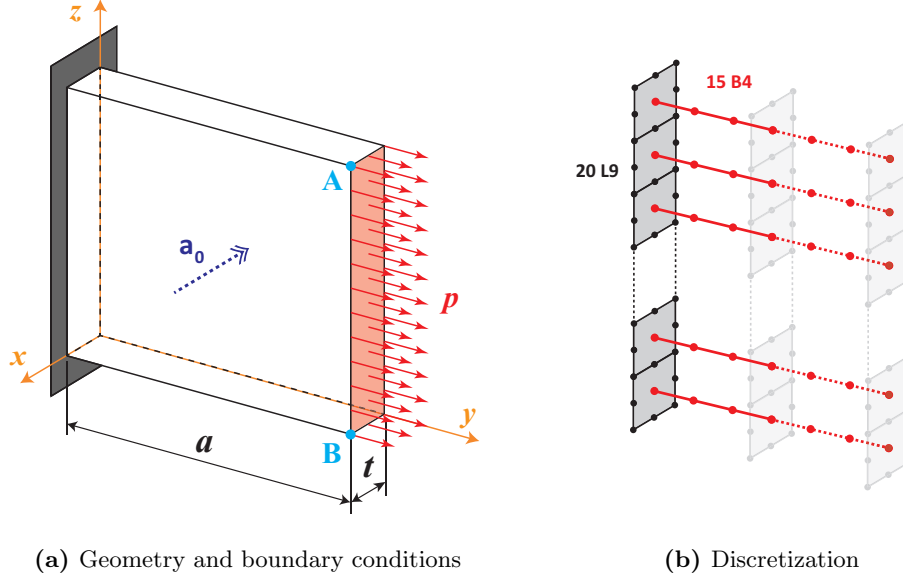**(a)** Geometry and boundary conditions        **(b)** Discretization

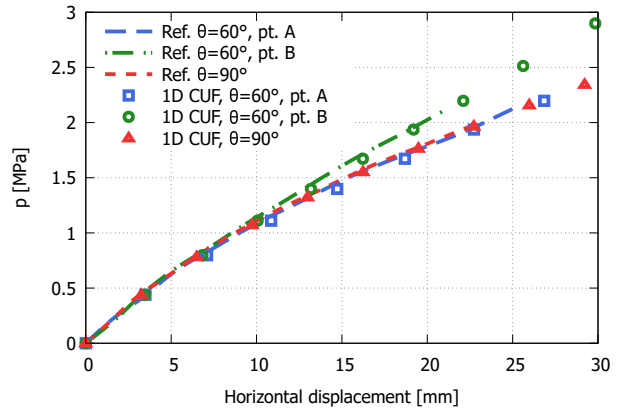**Figure 16:** Clamped square plate configuration of the case study

The square plate is made by a transversely isotropic hyperelastic material with a singe-fiber preferred direction, defined as the unitary vector $\mathbf{a_0}$ in the plane $y - z$ inclined of an angle $\theta$ with respect to $y$-axis, thus $\mathbf{a_0} = (0, \cos\theta, \sin\theta)$ the same plate is studied in different fiber configurations, with inclination angle varying from $0°$ to $90°$. Material is modeled adopting the same strain energy function model Eq.(56) of the previous case study, with the same material constants as done in the reference case [13].

The structure is discretized adopting 1D CUF models, employing 20 L9 parabolic elements along the clamped side of the plate and 15 B4 cubic elements along the longitudinal side of the beam in the $y$ direction as shown in Fig. 16(b), for a total number of degrees of freedom equal to 16974.

The effects of anisotropy and the presence of a preferential direction are investigated by analyzing the horizontal displacement of points A and B, located at the tip free-end of the plate, for increasing the value of the tensile traction load applied. Figure 17(a) shows the load-displacement curve for fiber inclination angle $\theta = 0°$ and $\theta = 30°$ in this case, for $\theta = 0°$ the horizontal displacement of the two-point are exactly coincident and, since the fiber direction is aligned with the load direction, the plate is much stiffer, instead in the case of $\theta = 30°$ there is a transversal component of the preferential direction that affects the deformation process, and the final configuration results unsymmetric. Figure 17(b) shows instead the equilibrium path curve for fiber inclination angle $\theta = 60°$ and $\theta = 90°$. Differently with respect to the previously considered cases, since the preferential direction is more inclined, the plate is much less stiff; large displacement and strains of the plate are obtained with much lower values of applied pressure. Again, when $\theta = 90°$ there is no component along the direction of the load thus the deformed structure is symmetric.
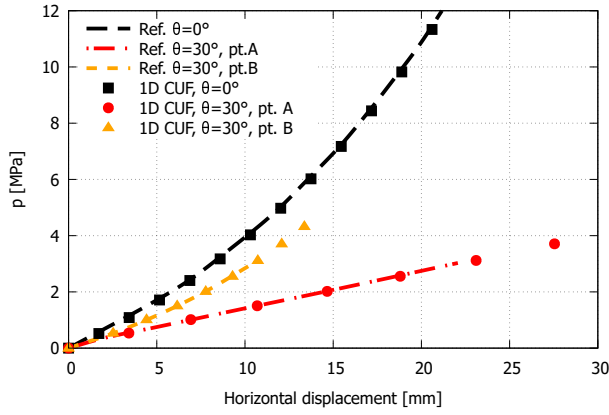
**(a)** Cases $\theta = 0°$ and $\theta = 30°$

**(b)** Cases $\theta = 60°$ and $\theta = 90°$

**Figure 17:** Clamped square plate equilibrium curve for various fiber inclination

Figure 18 shows the deformed configuration for different fiber inclination configurations when the horizontal displacement of the point $B$ is around 19 mm it can be clearly noted the strong influence of the mechanical behavior of the material with respect to anisotropy preferential direction.
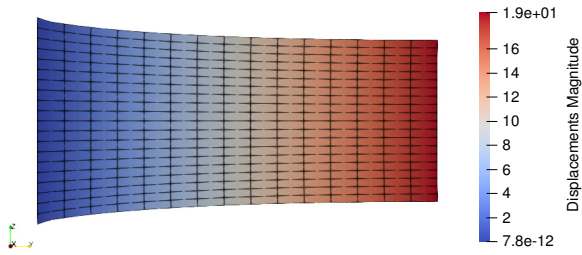


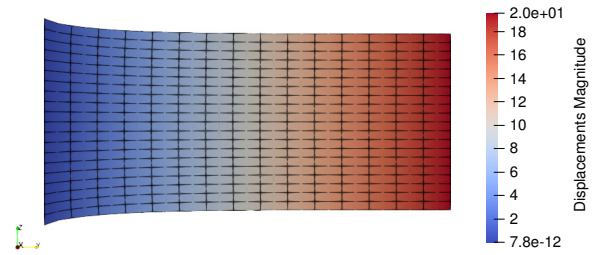**(a)** Fiber angle $\theta = 0°$
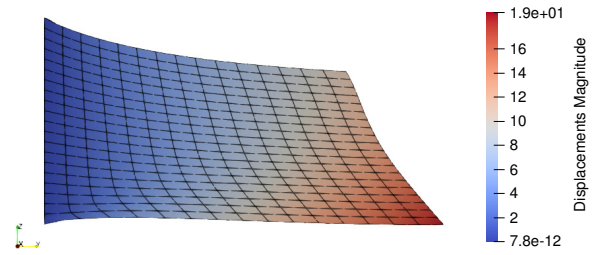
**(b)** Fiber angle $\theta = 30°$
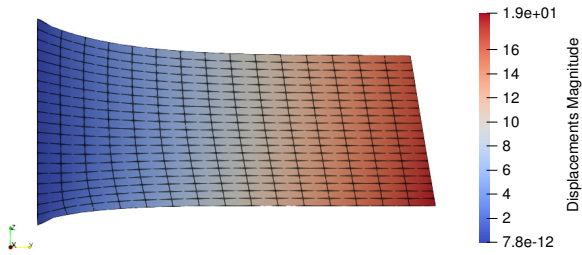
**(c)** Fiber angle $\theta = 60°$

**(d)** Fiber angle $\theta = 90°$

**Figure 18:** Clamped square plate deformed configuration representation

21

# 6 Conclusions

In this paper, we proposed the unified beam (1D) and plate (2D) CUF models for the large strain analysis of materials and structures in the hyperelastic compressible and incompressible regimes. In the domain of CUF, governing equations for the nonlinear static analysis of transversely isotropic hyperelastic materials are expressed in a compact notation starting from a generalized expansion of the 3D displacement unknowns coupling kinematic models and expansion theories, in a resulting expression of physical quantities (internal and external forces vector, tangent stiffness matrix) in matrix form, defining our fundamental nuclei independent of the polynomial expansion adopted. Numerical solutions are obtained by solving an algebraic system of equations with a Newton-Raphson linearized scheme. Our proposed results prove the capabilities of the present implementation of CUF 1D and 2D models to deal with large strains of fiber-reinforced hyperelastic structures, providing accurate results in terms of displacement and stress distributions, thanks to the higher-order three-dimensional description of the stress field guaranteed by the Unified formulation with adequate computational costs required for convergent solutions. The generalization of the constitutive law from isotropic hyperelastic to transversely isotropic hyperelastic materials is straightforward thanks to the Unified Formulation of tangent stiffness matrix in which the material Jacobian tensor is employed instead of the classical elasticity tensor, allowing us to rewrite the formulation of fully nonlinear finite element CUF models in the same framework without loss of generalities. Future works will deal with the extension of CUF hyperelastic models to shell structures, multilayered hyperelastic composites involved in biological tissue modeling (for which a suitable model for anisotropic behavior is required), the generalization of constitutive law adopted for orthotropic hyperelastic models in which the influence of two principal fiber directions are included, the stress analysis of multilayered composites made of linear elastic and hyperelastic layers, and finally the implementation of stabilization method for locking prevention, such as the *hybrid* formulation, in which the hydrostatic pressure (directly linked to the volumetric strains) is interpolated with an independent polynomial expansion.

# References

[1] Fok P-W. and Gou K. Finite element simulation of intimal thickening in 2d multi-layered arterial cross sections by morphoelasticity. *Computer Methods in Applied Mechanics and Engineering*, 363:112860, may 2020.

[2] Gerhard A. Holzapfel, Thomas C. Gasser, and Ray W. Ogden. A new constitutive framework for arterial wall mechanics and a comparative study of material models. *Journal of Elasticity*, 61(1/3):1–48, 2000.

[3] Fung Y.C., Fronek K., and Patitucci P. Pseudoelasticity of arteries and the choice of its mathematical expression. *American Journal of Physiology-Heart and Circulatory Physiology*, 237(5):H620–H631, nov 1979.

[4] Ogden R. W. Large deformation isotropic elasticity – on the correlation of theory and experiment for incompressible rubberlike solids. *Proceedings of the Royal Society of London. A. Mathematical and Physical Sciences*, 326(1567):565–584, feb 1972.

[5] Gent A. N. A new constitutive relation for rubber. *Rubber Chemistry and Technology*, 69(1):59–61, mar 1996.

[6] Puglisi G. and Saccomandi G. The gent model for rubber-like materials: An appraisal for an ingenious and simple idea. *International Journal of Non-Linear Mechanics*, 68:17–24, jan 2015.

[7] Arbind A., Reddy J.N., and Arun R. A general higher-order shell theory for compressible isotropic hyperelastic materials using orthonormal moving frame. *International Journal for Numerical Methods in Engineering*, 122(1):235–269, oct 2020.

[8] Amabili M., Breslavsky I.D., and Reddy J.N. Nonlinear higher-order shell theory for incompressible biological hyperelastic materials. *Computer Methods in Applied Mechanics and Engineering*, 346:841–861, apr 2019, DOI: 10.1016/j.cma.2018.09.023.

[9] Amabili M., Balasubramanian P., Bozzo I., Breslavsky I.D., and Ferrari G. Layer-specific hyperelastic and viscoelastic characterization of human descending thoracic aortas. *Journal of the Mechanical Behavior of Biomedical Materials*, 99:27–46, nov 2019, DOI: 10.1016/j.jmbbm.2019.07.008.

[10] Balzani D., Gruttmann F., and Schröder J. Analysis of thin shells using anisotropic polyconvex energy densities. *Computer Methods in Applied Mechanics and Engineering*, 197(9-12):1015–1032, feb 2008.

[11] Brown L.W. and Smith L.M. A simple transversely isotropic hyperelastic constitutive model suitable for finite element analysis of fiber reinforced elastomers. *Journal of Engineering Materials and Technology*, 133(2), mar 2011.

[12] Canales C., Garcia-Herrera C., Rivera E., Macias D., and Celentano D. Anisotropic hyperelastic material characterization: Stability criterion and inverse calibration with evolutionary strategies. *Mathematics*, 11(4):922, feb 2023.

[13] Beheshti A and Ansari R. Finite element analysis of compressible transversely isotropic hyperelastic shells. *Acta Mechanica*, mar 2023.

[14] Zdunek A. and Rachowicz W. A mixed higher order FEM for fully coupled compressible transversely isotropic finite hyperelasticity. *Computers & Mathematics with Applications*, 74(7):1727–1750, oct 2017.

[15] Carrera E., Cinefra M., Zappino E., and Petrolo M. *Finite Element Analysis of Structures Through Unified Formulation*. Wiley, Wiley, Chichester, West Sussex, UK, jul 2014.

[16] Carrera E., Cinefra M., and Li G. Refined finite element solutions for anisotropic laminated plates. *Composite Structures*, 183:63–76, jan 2018, DOI: 10.1016/j.compstruct.2017.01.014.

[17] Cinefra M., Chinosi C., Croce L.D., and Carrera E. Refined shell finite elements based on RMVT and MITC for the analysis of laminated structures. *Composite Structures*, 113:492–497, jul 2014, DOI: 10.1016/j.compstruct.2014.03.039.

[18] Carrera E. and Cinefra M. Classical, refined, zig-zag and layer-wise models for laminated structures. In *Computational and Experimental Methods in Structures*, pages 135–172. Imperial College Press, nov 2013, DOI: 10.1142/9781848167858_0004.

[19] Pagani A. and Carrera E. Unified formulation of geometrically nonlinear refined beam theories. *Mechanics of Advanced Materials and Structures*, 25(1):15–31, sep 2016.

[20] B. Wu, A. Pagani, M. Filippi, W.Q. Chen, and E. Carrera. Large-deflection and post-buckling analyses of isotropic rectangular plates by carrera unified formulation. *International Journal of Non-Linear Mechanics*, 116:18–31, nov 2019.

[21] Carrera E., Pagani A., and Augello R. Large deflection of composite beams by finite elements with node-dependent kinematics. *Computational Mechanics*, 69(6):1481–1500, mar 2022.

[22] Pagani A. and Carrera E. Unified one-dimensional finite element for the analysis of hyperelastic soft materials and structures. *Mechanics of Advanced Materials and Structures*, pages 1–14, dec 2021.

[23] Augello R., Carrera E., Filippi M., Pagani A., and Tortorelli E. Unified plate finite elements for the large strain analysis of hyperelastic material structures. *International Journal of Non-Linear Mechanics*, page 104465, jun 2023.

[24] Pagani A., Chiaia P., Filippi M., and Cinefra M. Unified three-dimensional finite elements for large strain analysis of compressible and nearly incompressible solids. *Submitted to Mechanics of Advanced Materials and Structures, accepted under revision*, 2023.

[25] Holzapfel G.A. *Nonlinear Solid Mechanics*. John Wiley & Sons, Chichester, West Sussex, UK, 2000.

[26] Carrera E., Giunta G., and Petrolo M. *Beam Structures Classical and Advanced Theories*. Wiley, Chichester, West Sussex, UK, 2011.

[27] Carrera E., Pagani A., Augello R., and Wu B. Popular benchmarks of nonlinear shell analysis solved by 1d and 2d CUF-based finite elements. *Mechanics of Advanced Materials and Structures*, 27(13):1098–1109, feb 2020, DOI: 10.1080/15376494.2020.1728450.

[28] Pagani A., Daneshkhah E., Xu X., and Carrera E. Evaluation of geometrically nonlinear terms in the large-deflection and post-buckling analysis of isotropic rectangular plates. *International Journal of Non-Linear Mechanics*, 121:103461, may 2020, DOI: 10.1016/j.ijnonlinmec.2020.103461.

[29] Carrera E., Pagani A., Giusa D., and Augello R. Nonlinear analysis of thin-walled beams with highly deformable sections. *International Journal of Non-Linear Mechanics*, 128:103613, jan 2021, DOI: 10.1016/j.ijnonlinmec.2020.103613.

[30] Reddy J. N. *Introduction to Nonlinear Finite Element Analysis With Applications to Heat Transfer, Fluid Mechanics, and Solid Mechanics*. Oxford University Press, 2014.

[31] Crisfield M.A. An arc-length method including line searches and accelerations. *International Journal for Numerical Methods in Engineering*, 19(9):1269–1289, sep 1983.

[32] Carlos Castillo-Méndez and Armando Ortiz. Role of anisotropic invariants in numerically modeling soft biological tissues as transversely isotropic hyperelastic materials: A comparative study. *International Journal of Non-Linear Mechanics*, 138:103833, jan 2022.